Expression and biophysical properties of Kv1 channels in supragranular neocortical pyramidal neurones

D. Guan[1], J. C. F. Lee[1], T. Tkatch[2], D. J. Surmeier[2], W. E. Armstrong[1] and R. C. Foehring[1]

[1] *Department of Anatomy and Neurobiology, University of Tennessee, 855 Monroe Avenue, Memphis, TN 38163, USA*
[2] *Department of Physiology, Northwestern University, 745 N. Fairbanks Court, Chicago, IL 60611, USA*

Potassium channels are extremely diverse regulators of neuronal excitability. As part of an investigation into how this molecular diversity is utilized by neurones, we examined the expression and biophysical properties of native Kv1 channels in layer II/III pyramidal neurones from somatosensory and motor cortex. Single-cell RT-PCR, immunocytochemistry, and whole cell recordings with specific peptide toxins revealed that individual pyramidal cells express multiple Kv1 α-subunits. The most abundant subunit mRNAs were Kv1.1 > 1.2 > 1.4 > 1.3. All of these subunits were localized to somatodendritic as well as axonal cell compartments. These data suggest variability in the subunit complexion of Kv1 channels in these cells. The α-dendrotoxin (α-DTX)-sensitive current activated more rapidly and at more negative potentials than the α-DTX-insensitive current, was first observed at voltages near action potential threshold, and was relatively insensitive to holding potential. The α-DTX-sensitive current comprised about 10% of outward current at steady-state, in response to steps from −70 mV. From −50 mV, this percentage increased to ∼20%. All cells expressed an α-DTX-sensitive current with slow inactivation kinetics. In some cells a transient component was also present. Deactivation kinetics were voltage dependent, such that deactivation was slow at potentials traversed by interspike intervals during repetitive firing. Because of its kinetics and voltage dependence, the α-DTX-sensitive current should be most important at physiological resting potentials and in response to brief stimuli. Kv1 channels should also be important at voltages near threshold and corresponding to interspike intervals.

(Received 19 August 2005; accepted after revision 21 December 2005; first published online 22 December 2005)
Corresponding author R. C. Foehring: Department of Anatomy and Neurobiology, University of Tennessee, 855 Monroe Avenue, Memphis, TN 38163, USA. Email: rfoehrin@utmem.edu

Potassium channels are extremely diverse due to numerous gene families, multiple genes per family, heteromultimeric combination of subunits, auxiliary subunits, splice variants, and post-translational processing (Salkoff *et al.* 1992; Coetzee *et al.* 1999). How is this potential molecular diversity used by neurones to regulate excitability? To address this question, we investigated the expression and biophysical properties of Kv1 channels in supragranular pyramidal cells from neocortex.

Kv1 α-subunits are the mammalian homologues of *Drosophila* Shaker subunits (Stuhmer *et al.* 1989; Jan & Jan, 1992). At least six members of this family have been described in the brain (Kv1.1–1.6: Coetzee *et al.* 1999; Coghlan *et al.* 2001) and the Kv1 genes show region- and cell type-specific expression (Baldwin *et al.* 1991; Drewe *et al.* 1992; Hwang *et al.* 1992; Rettig *et al.* 1994; Sheng *et al.* 1992; Tsaur *et al.* 1992; Veh *et al.* 1995). In cortex, immunocytochemical studies suggest that Kv1.1 subunits are found throughout the neuropil and on the somas of pyramidal cells, especially in layer V (Wang *et al.* 1994). Kv1.2 subunits are also found throughout the neuropil and in the apical dendrites of pyramidal cells (Sheng *et al.* 1994), with little staining of somas (Wang *et al.* 1994). Kv1.4 subunits were also found in cortical neuropil (Sheng *et al.* 1992; Cooper *et al.* 1998), suggesting an axonal/terminal distribution. Lujan *et al.* (2003) described Kv1.4 immunoreactivity in the neuropil, with additional staining of dendrites and somas of pyramidal cells (layer V > layers II/III).

Kv1 subunits can form heteromultimeric channels *in vitro* (Salkoff *et al.* 1992; Po *et al.* 1993; Rettig *et al.* 1994; Heineman *et al.* 1996). Furthermore, coimmunoprecipitation experiments have revealed *in vivo* associations of Kv1.2 with Kv1.4 (Sheng *et al.* 1993), Kv1.1 with Kv1.2 (Wang *et al.* 1993), and Kv1.2 with Kv1.3 (Sheng *et al.* 1994). On the basis of such studies, it has been proposed that all Kv1-containing channels in cortex are heteromultimeric (Shamotienko *et al.* 1997; Coleman *et al.* 1999; Wang *et al.* 1999). Aditional channel heterogeneity is generated by association of Kvβ subunits with Kvα subunits. Kvβ1 and Kvβ2 have been shown to colocalize

 DOI: 10.1113/jphysiol.2005.097006

and associate with Kv1.1, Kv1.2, Kv1.4, Kv1.6 and Kv2.1 α subunits (Sheng *et al.* 1993; Rhodes *et al.* 1997; Shamotienko *et al.* 1997).

With the exception of Kv1.4, Kv1 channels form slowly inactivating currents when expressed as homomeric channels in heterologous systems (Serodio & Rudy, 1998; Stuhmer *et al.* 1989; Tseng-Crank *et al.* 1990; Pongs, 1992; Jan & Jan, 1992; Po *et al.* 1993). In contrast, homomeric Kv1.4 channels form a rapidly inactivating A-type current. Other Kv1 subunits can also form channels with transient currents when combined with auxiliary Kvβ1 subunits (Rettig *et al.* 1994; Castellino *et al.* 1995; Morales *et al.* 1995). At present, we have limited knowledge about the subunit composition or specific roles of native channels.

α-Dendrotoxin (α-DTX), a peptide from the venom of mamba snakes (*Dendroaspis*), is frequently used to isolate Kv1 currents due to the Kv1.1, Kv1.2 and Kv1.6 α subunits. α-DTX-sensitive currents have been recorded in many cell types, including neocortical (Foehring & Surmeier, 1993; Zhou & Hablitz, 1996; Locke & Nerbonne, 1997; Korngreen & Sakmann, 2000; Bekkers & Delaney, 2001; Dong & White, 2003) and hippocampal (Halliwell *et al.* 1986; Wu & Barish, 1992; Bossu & Gahwhiler, 1996; Chen & Johnston, 2004) pyramidal cells. The α-DTX-sensitive currents show considerable variability in properties across cell types, however, perhaps due to diverse subunit compositions (Coetzee *et al.* 1999).

The function of Kv1 channels has been particularly well illustrated in cells within the auditory system, where high densities of Kv1 channels facilitate selectivity for time varying stimuli, rather than DC inputs (Brew & Forsythe, 1995; Dodson *et al.* 2002; Rothman & Manis, 2003*a*,*b*,*c*). Because Kv1 channels activate in the subthreshold voltage range in many cell types (Bekkers & Delaney, 2001; Dodson *et al.* 2002; Shen *et al.* 2004) they are likely to play an important role in regulating cell excitability. Kv1.1 knockout mice are subject to seizures (Smart *et al.* 1998; Rho *et al.* 1999), although only modest physiological changes were reported (Smart *et al.* 1998; van Brederode *et al.* 2001).

We examined the following questions. (1) Which Kv1 subunits are expressed in neocortical layer II/III pyramidal neurones? (2) Do these channels exist as heteromeric complexes? (3) What are the biophysical properties of the α-DTX-sensitive current?

Methods

These studies were performed on juvenile rats (Sprague-Dawley, P28–35). All procedures were approved by the Animal Care and Use Committee, University of Tennessee, Health Science Center. The animals were anaesthetized with isofluorane until the animal was areflexive. Briefly, the animal was placed into a sealed plastic container into which gauze soaked with isofluorane was placed under a fibreglass screen floor. After anaesthesia with isoflurane, the animals were decapitated, and the brain was removed and dropped into ice cold cutting solution for 30–60 s. The cutting solution contained (mM): 250 sucrose, 25 KCl, 1 NaH_2PO_4, 11 glucose, 4 $MgSO_4$, 0.1 $CaCl_2$, 15 Hepes (2-bis(2-aminophenoxy)ethane-*N*,*N*,*N*′,*N*′-tetraacetic acid) (pH = 7.3–7.4; 300 mosmol l^{-1}).

We made 400 μm coronal slices of the fronto-parietal regions of the brain using a vibrating tissue slicer (World Precision Instruments, Sarasota, FL, USA). The slices were then transferred to a mesh surface in a chamber containing artificial cerebrospinal fluid (aCSF) at room temperature. The aCSF contained (mM): 125 NaCl, 3 KCl, 2 $CaCl_2$, 2 $MgCl_2$, 1.25 NaH_2PO_4, 26 $NaHCO_3$, and 20 glucose (pH 7.4, 310 mosmol l^{-1}), and was bubbled with a 95% O_2–5% CO_2 (carbogen) mixture.

Acute isolation of neurones

Just prior to enzyme treatment, the combined primary motor and primary somatosensory cortices were dissected from brain slices under a stereomicroscope. The cortex was further cut to restrict enzyme treatment to the supragranular layers (I/III). Two to three cortex pieces at a time were transferred to oxygenated aCSF (35°C) with added enzyme (Sigma Protease type XIV, 1.2 mg ml^{-1}: Sigma Chemicals, St Louis, MO, USA). After 20–30 min of incubation in enzyme, the tissue was washed with sodium isethionate solution, which consisted of (mM): 140 sodium isethionate, 2 KCl, 4 $MgCl_2$, 23 glucose, 15 Hepes, pH 7.3 (adjusted with 1 M NaOH).

This solution and enzyme-treated tissue were triturated using three successively smaller fire-polished pipettes to release individual neuronal somata. The supernatant from each trituration step (containing dissociated neurones) was transferred to a fresh container, plated onto a plastic Petri dish (Nunc, Rochester, NY, USA) on an inverted microscope stage, and allowed to settle for approximately 5 min. A background flow of ~1 ml min^{-1} of Hepes-buffered saline solution (HBSS) was then established. HBSS consisted of (mM): 138 NaCl, 3 KCl, 1 $MgCl_2$, 2 $CaCl_2$, 10 Hepes, 10–20 dextrose, pH 7.3 (adjusted with 1 N NaOH), and osmolarity = 300–305 mosmol l^{-1}. The external recording solution was HBSS, plus tetrodotoxin (TTX: 1 μM) and $CdCl_2$ (400 μM) to block Na^+ and Ca^{2+} channels, respectively.

Corning 7052 capillary glass (Garner Glass: Claremont, CA, USA) was used to create electrodes on a Sutter Instruments (Novato, CA, USA) Model P-87 Flaming/Brown micropipette puller. Electrodes were fire-polished and filled with internal solution. Two internal solutions were used (no differences were observed

in the recorded currents between the two internals). The first consisted of (mM): 120 $KMeSO_4$, 15 KOH, 2 $MgCl_2$, 7.5 NaCl, 30 Hepes, 2 adenosine 5′-triphosphate (ATP), 0.2 guanosine 5′-triphosphate (GTP), 0.1 leupeptin, 1–10 2-bis(2-aminophenoxy)ethane-*N*,*N*,*N*′,*N*′-tetraacetic acid (BAPTA). The second internal solution contained 75 $KMeSO_4$, 60 KOH, 2 $MgCl_2$, 7.5 NaCl, 40 Hepes, 2 ATP (Na^+ salt), 0.2 GTP, 0.1 leupeptin, 10 BAPTA. Both internals were ∼270 mosmol l^{-1} and adjusted to pH 7.2 with KOH.

A multibarrel array of glass capillaries (∼500 μm outer diameter) in 'sewer pipe' configuration was used to apply solutions. Six capillaries were glued side to side and attached to a micromanipulator. Solutions were changed by moving the active barrel so that the flow surrounded the recorded cell. Care was taken to regulate flow through the array to prevent flow artifacts. The following channel blockers (Alomone Laboratories, Ltd, Jerusalem, Israel) were used: TTX (1 μM), $CdCl_2$ (400 μM), α-dendrotoxin (0.1–1000 nM), δ-dendrotoxin (10 nM), dendrotoxin-K (10–100 nM), r-tityustotoxin-Kα (100 nM), r-margatoxin (1–30 nM).

Recordings were made with a Dagan 8900 (Minneapolis, MN, USA) amplifier at room temperature (21–23°C). Electrode resistances were 1.4–2.2 MΩ after polishing, and series resistance compensation was 70–90%. For experiments detailing voltage dependence and kinetics of currents, cells with calculated series resistance errors of ≥ 5 mV were discarded (($V = IR$): series resistance error (V) = remaining series resistance after compensation (R) multiplied by peak current (I)). Data were acquired using pCLAMP 8. Reported membrane potentials were corrected off-line for the measured liquid junctional potential (∼8 mV). Data acquisition (20 kHz sampling, filtered at 5 kHz) and analysis were done using pCLAMP and Axograph software (Axon Instruments, Union City, CA, USA). Linear leak current and the capacitative artifact were digitally subtracted before analysis, using a *P*/4 protocol.

RT-PCR

Cell harvest. Acutely dissociated neurones were used for these experiments. Sterile gloves were worn at all times in this and subsequent steps to minimize RNAase contamination. Pyramidal neurones were initially identified by shape and the presence of an apical dendrite. Electrode glass (Corning 7052) was autoclaved and heated to 150–200°C for 2 h. After formation of a gigaohm seal, the cell was lifted up into a stream of HBSS. Suction was increased under visual control until the cell was aspirated into the pipette. The pipette contained diethylpyrocarbonate (DEPC)-treated water and 0.8 U ml^{-1} Superase-IN (Ambion, Austin, TX, USA). After aspiration, the electrode containing the cell was broken into a 0.6 ml presiliconized Midwest Scientific tube (Valley Park, MO, USA) and the contents ejected into the cell collection components for reverse transcription (see below). Five to ten cells were harvested per experiment and the cells/collection components were subjected to the reverse transcriptase (RT) procedure.

Tissue and single cell RT-PCR (scRT-PCR) analysis. Eppendorf tubes containing 0.7 μl of Superase-IN (20 U μl^{-1}), 1.9 μl of DEPC-treated water, 1 μl of dNTPs (10 mM), 0.7 μl of BSA (143 $\mu g\,\mu l^{-1}$), and 0.7 μl of oligo-dT (0.5 $\mu g\,\mu l^{-1}$) together with cell content were heated to 65°C for 5 min and then placed on ice for at least 1 min. Single-strand cDNA was synthesized from the cellular mRNA by adding 2 μl of 10× PCR buffer, 4 μl of $MgCl_2$ (25 mM), 2 μl of DTT (0.1 M), 1 μl of RNAase Out (40 U μl^{-1}), 1 μl of Superscript III (50 U μl^{-1}) and 6 μl of DEPC-treated water. The RT was then incubated at 50°C for 90 min. The reaction was terminated by heating the mixture to 85°C for 5 min. The RNA strand in the RNA–DNA hybrid was then removed by adding 0.5 μl of RNase H (2 U μl^{-1}) and incubated at 37°C for 20 min. All reagents except Superase-IN (Ambion) were obtained from Invitrogen (Gaithersburg, MD, USA). The tubes were then placed on ice and shipped overnight to Dr Surmeier's lab at Northwestern University.

PCR. PCR was performed (at Northwestern University) using procedures designed to minimize cross-contamination. Negative controls for contamination from extraneous (replacing cellular template with water) and genomic DNA (without reverse transcriptase) were run for every batch of neurones. The single cell cDNA generated from the above step was subjected to conventional PCR using a programmable thermal cycler. PCR primers were developed from the GenBank sequences with OLIGO software (v6.6). Primers were for calcium–calmodulin kinase II (CamKII), Kv1.1, 1.2, 1.3, 1.4, 1.5 and 1.6. Primers for Kv1.2, 1.3 and 1.6 are published in Shen *et al.* (2004); for Kv1.5, Song *et al.* (1998); and for CamKII, Vysokanov *et al.* (1998). CamKII was used as a marker for pyramidal neurones (Jones *et al.* 1994). 'Touchdown' protocols were implemented for more efficient amplification of single cell DNA: 35 cycles were run at the optimal annealing temperature for each primer set, then the annealing temperature was decreased by 1 for two cycles –five times – for a total of 45 cycles.

Immunocytochemistry. Animals were anaesthetized with sodium pentobarbital (50 mg kg^{-1} I.P.). The anaesthetized animals were transcardially perfused with 0.01 M sodium phosphate buffer plus 0.89% NaCl (PBS) for exsanguination, followed by PBS buffered 4%

paraformaldehyde and 0.2% picric acid. The brain was removed and stored for ∼12 h in fixative. At this point, a transverse cut was made to improve access of the fixative to the brain ventricular system and sucrose was added to the fixative (30% weight/volume) for cryoprotection. The brain was maintained in the sucrose/fixative mixture for 1–10 days. The brain was sectioned at 40 μm on a freezing microtome.

Sections were incubated in 2% normal goat serum with 3% H_2O_2 for 1–2 h to reduce background staining. Several antibodies (rabbit polyclonal: Kv1.1, 1.2, 1.3, 1.4, 1.5, 1.6) were obtained from Alomone Laboratories (Jeruselem, Israel) and dissolved at various concentrations (1 : 100 to 1 : 1000) in PBS and 0.5% Triton X-100 (PBS-TX). For antibodies generating positive results, a further test for specificity utilized a separate set of sections, which were incubated in the subunit peptide provided by Alamone for absorption. Additional monoclonal antibodies (Kv1.1, Kv1.2) were obtained from Upstate (Waltham, MA, USA). The monoclonal Kv1.3 antibody was a gift from J. Trimmer. After three 10 min rinses in PBS, the sections were incubated for 24–48 h in PBS-TX with the antibody (4°C).

After three rinses with PBS-TX, the sections were incubated in biotinylated goat anti-rabbit (GAR-B) or horse anti-mouse (HAM-B) at 1 : 200 overnight (4°C). After three rinses in PBS-TX, the sections were incubated for ∼4 h with Avidin-Biotin-Peroxidase (ABC: Vector Laboratories) dissolved in PBS-TX. After three rinses in PBS-TX, the sections were reacted (per Vector protocol) with Ni^{2+}-intensified DAB (60 mg ml^{-1}) plus 0.003% H_2O_2 for 5–10 min. The reaction was terminated by several rinses in PBS-TX. The sections were then mounted on gel-coated glass slides, dehydrated and coverslipped.

Statistics

Prism (GraphPad Software, Inc., San Diego, CA, USA) was used for statistical tests of significance. Student's paired or unpaired *t* test was used to compare sample population data throughout, and summary data are presented as means ± standard deviation, unless noted otherwise. $P = 0.05$ was taken as the level of significance.

Sample population data are represented as scatter plots or as box plots (Tukey, 1977). Box plots indicate the upper and lower quartiles as edges of the box, with the median represented as a line crossing the box. The stems indicate the smallest and lowest non-outlying values, and outliers are indicated by open circles. Outlying values are greater than 1.5 times the quartile boundaries.

Results

We first tested which Kv1 subunits were expressed in layer II/III pyramidal neurones from motor and somatosensory cortex using single cell RT-PCR, immunocytochemistry, and a combination of whole cell recording with subunit-specific peptide blockers.

mRNA

Single cell RT-PCR was performed on cells from juvenile animals (4–5 weeks postnatal) to profile mRNA expression in individual layer II/III pyramidal cells. Cells were initially identified as pyramidal by the presence of a single, dominant apical dendrite. Care was taken to ensure that only the contents of a single cell was harvested (see Methods). A final test for pyramidal cell identity was use of a primer for Ca^{2+}–calmodulin kinase II (CamKII), a specific marker for a subset of pyramidal cells in cortex (Jones *et al.* 1994). RT-PCR was performed using four of the six Kv1 primers per cell. We varied the particular combinations of Kv1 primers (Fig. 1).

We detected Kv1 mRNAs in 61/64 cells tested (7 animals) (Fig. 1*A* and *B*). Kv1.1 was the most commonly observed mRNA, being present in 85% (40/47) of the cells. Kv1.2 mRNA was observed in 68% (32/47) of the cells, Kv1.3 in 40% (19/47), Kv1.4 in 60% (27/45), Kv1.5 in 14% (5/37), and Kv1.6 in 31% (11/36). Most (47/64 = 73%) cells expressed two or more Kv1 mRNAs, with 44% expressing two, 22% expressing three, and 8% expressing four mRNAs (Fig. 1*C*). These data should be considered underestimates of coexpression, since only four of six mRNAs could be tested in a single cell. We detected all combinations of two subunits except for Kv1.3 + Kv1.5 and Kv1.3 + Kv1.6. The most commonly observed combinations of two subunits were Kv1.1 + Kv1.2 (41%), Kv1.2 + Kv1.3 (25%), Kv1.1 + Kv1.3 (20%), Kv1.1 + Kv1.4 (19%), and Kv1.2 + Kv1.4 (13%).

Immunocytochemistry

The mRNA data indicated that most layer II/III pyramidal cells express multiple Kv1 mRNAs. We next used immunocytochemistry to determine whether the corresponding proteins were expressed and if so, in which cell compartments. Our initial experiments used polyclonal antibodies from Alomone Laboratories, with variable success. Results were considered positive when staining was absent after preincubation with the corresponding peptide and when consistent results were obtained in two or more animals. We saw almost no labelling in cortex with the Kv1.5 and Kv1.6 antibodies, consistent with their low incidence of expression for mRNA. The most consistent results were obtained with the Kv1.1 (Fig. 2*A*) and Kv1.4 (Fig. 2*B*) antibodies. The Kv1.1 antibody intensely stained neuropil in all layers. In addition, Kv1.1 was observed in apical dendrites and somas of some layer II/III pyramidal cells (Fig. 2*A*). Kv1.4 showed a very similar pattern to Kv1.1, staining dendrites and somas of pyramidal neurones (Fig. 2*B*), as well as the surrounding neuropil. For both

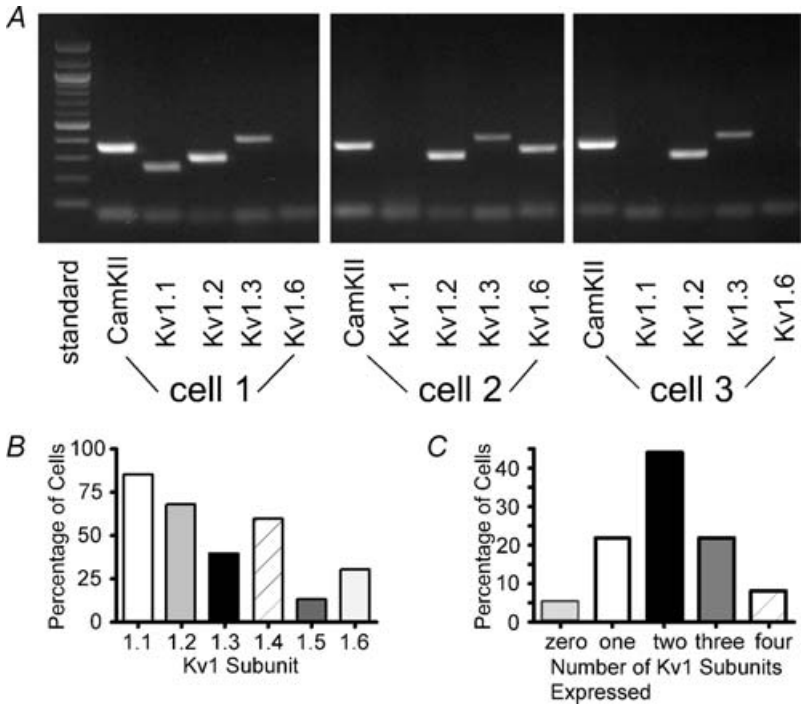

Figure 1. Kv1 mRNA expression in layer II/III pyramidal neurones from rat somatosensory and motor cortex
A, representative gel for three different cells. All cells expressed CamKII (marker for pyramidal neurones: Jones *et al.* 1994). Cell 1 expressed Kv1.1, Kv1.2 and Kv1.3, but not Kv1.6. Cell 2 expressed Kv1.2, Kv1.3 and Kv1.6 (not Kv1.1). Cell 3 expressed Kv1.2 and Kv1.3 (not Kv1.1 or Kv1.6). *B*, bar graph indicating percent of cells expressing each subunit. *C*, bar graph showing the percentage of cells that expressed each number of subunits.

Kv1.1 and Kv1.4, more cells were labelled in layer V than in layers II/III and staining was more intense in motor and cingulate cortex than in somatosensory cortex (data not shown). We did not obtain consistent results with the Alamone Kv1.2 or Kv1.3 antibodies (see also Dodson *et al.* 2003).

Both the Kv1.1 (not shown) and 1.2 antibodies (Fig. 3*A*) from Upstate consistently labelled neuropil in all cortical layers. The Kv1.1 results were similar to the Alamone antibody (Fig. 3*A*; cf. Wang *et al.* 1993; Monaghan *et al.* 2001), although the antibody also stained the nucleus, in addition to soma, dendrites and neuropil. Staining with the Kv1.2 antibody (Fig. 3*A*) was relatively homogeneous, staining neuropil as well as apical dendrites and soma. This was especially true in layers II/III (Fig. 3*A*1). In layer V (Fig. 3*A*2), the Kv1.2 antibody stained neuropil, the dendrites of pyramidal cells and a few somas. The staining in some areas appeared to surround the soma as if

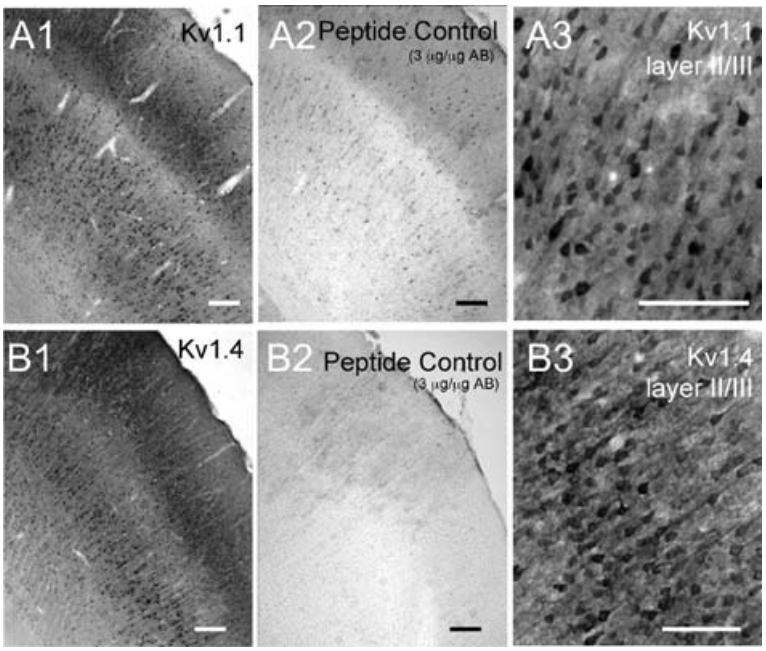

Figure 2. Immunohistochemical expression of Kv1.1 and Kv1.4
Polyclonal antibodies were obtained from Alamone Laboratories. Both antibodies stained the neuropil in all cortical layers. Scale bars = 100 μm. *A*, Kv1.1 antibody. *A*1, low power (4×) view of somatosensory cortex illustrating staining in pyramidal cell layers II/III and V. Note relative lack of labelling in layer IV. *A*2, pretreatment with absorption peptide eliminated staining. *A*3, higher power (20×) view of layer II/III showing staining of somas of pyramidal neurones. *B*, Kv1.4 antibody. *B*1, low power (4×) view of somatosensory cortex illustrating staining in pyramidal cell layers II/III and V. Note relative lack of labelling in layer IV. *B*2, pretreatment with absorption peptide eliminated staining. *B*3, higher power (20×) view of layer II/III showing staining of somas and apical dendrites of pyramidal neurones.

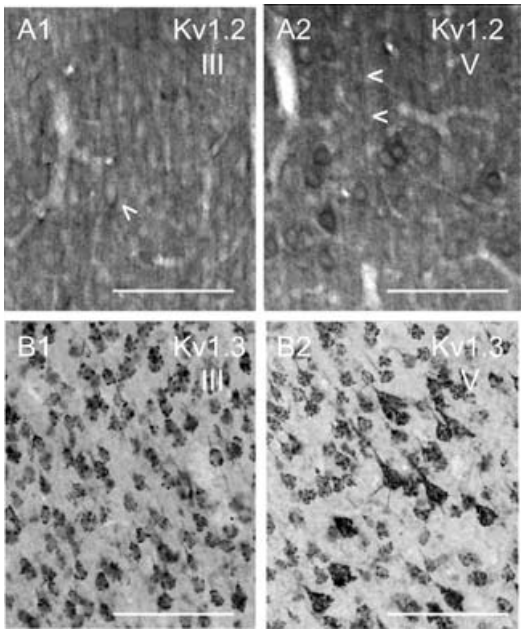

Figure 3. Immunohistochemical expression of Kv1.2 and Kv1.3
The monoclonal Kv1.2 antibody (A) was obtained from Upstate (Waltham, MA, USA). The monoclonal Kv1.3 antibody (B) was a gift from Dr J. Trimmer. Scale bars = 100 μm. *A*, monoclonal antibody to Kv1.2. *A*1, layer III of somatosensory cortex (20×), showing relatively homogeneous staining of neuropil, as well as apical dendrites and perisomatic staining (arrowhead). *A*2, layer V (20×) showing staining of apical dendrites of pyramidal cells (note arrowheads), as well as perisomatic staining of pyramidal cells. *B*, monoclonal antibody to Kv1.3. *B*1, layer III of of somatosensory cortex (20×), showing the grape-like punctate pattern of staining over somas/proximal dendrites. *B*2, layer V (20×) showing the grape-like cluster pattern of staining over somas/proximal dendrites.

presynaptic terminals were stained (see also Wang *et al.* 1993; Sheng *et al.* 1994).

We also obtained consistent results with a monoclonal antibody to Kv1.3 obtained from Dr J. Trimmer (University of California, Davis; Fig. 3*B*). This antibody labelled neuropil in cortex and there was extensive staining in layers II/III and V of motor and somatosensory cortex. The staining was punctate over pyramidal cell somata (Fig. 3*B*). We did not have a peptide control for the Kv1.3 antibody.

Recordings of K^+ currents

Rundown. In the absence of pharmacological intervention, currents are typically stable from break-in until about 3–5 min into the recording, after which the currents run down (data not shown). The average rate of run down in a random sample of 18 recordings was 87 ± 90 pA min^{-1} (range 4–343 pA min^{-1}). Subtraction of currents obtained at later time points from the initial current revealed that the 'run-down' current activated very slowly (data not shown), unlike the current sensitive to α-DTX (e.g. Figs 4*D* and 6*A* and *D*). Subsequent experiments were therefore designed to gather data within the stable period and cells with obvious run-down were discarded. For cells included in further analyses, rundown ranged between 4 and 150 pA min^{-1}.

α-Dendrotoxin-sensitive current. In expression systems, α-dendrotoxin (α-DTX) blocks current through channels composed of Kv1.1, 1.2 or 1.6 subunits (K_D: 1–25 nM; Harvey & Robertson, 2004). We tested for functional α-DTX-sensitive currents in acutely dissociated layer II/III pyramidal neurones (Fig. 4). A 200 ms test voltage step from the holding potential (−70 mV) to +10 mV was repeated every 5 s. After currents were stable in control solution, we switched to a solution containing 100 nM α-DTX. We observed a measurable α-DTX-sensitive current in 42/45 cells tested with this protocol (Fig. 4*A*). The block by α-DTX was rapid and partially reversible, with a τ_{block} of 9.5 ± 7.8 s (Fig. 4*B*; $n = 20$ cells). With this protocol, 100 nM α-DTX blocked 11.1 ± 5.1% at the peak current (8.8 ± 5.1% of the current at 200 ms: Table 1,

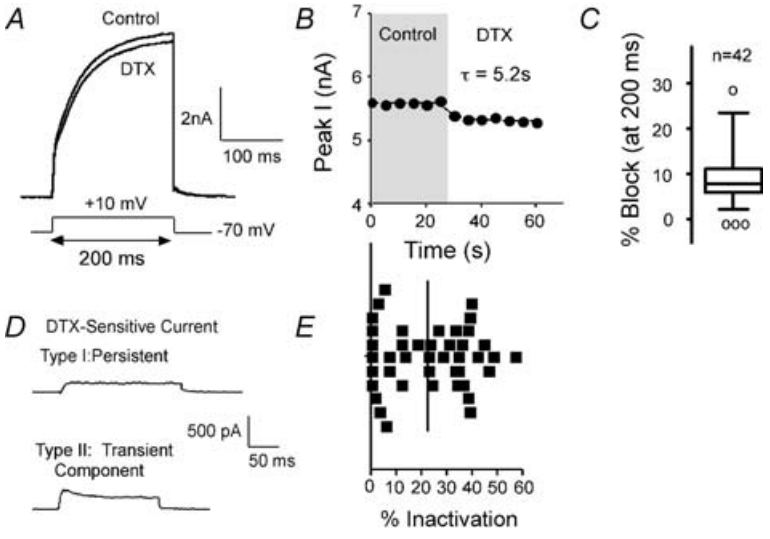

Figure 4. Currents sensitive to α-dendrotoxin (α-DTX)
A, α-DTX (DTX) blocked a portion of the current elicited by steps to +10 mV from −70 mV. *B*, plot of current *versus* time for cell shown in *A*. The effect of α-DTX was rapid (τ of 5.2 s in this cell). *C*, box plot shows variability in response to α-DTX in 42 cells (test step as in *A*). Line in box indicates median. Outer edges of box represent inner quartile and whiskers indicate outer quartile for data. ○, outliers (Tukey, 1977). *D*, examples of α-DTX-sensitive currents (at +10 mV) from two different cells. The upper cell showed rapid activation and little inactivation over the 200 ms step. The lower cell exhibited both transient and persistent components. *E*, scatter plot shows distribution of percentage inactivation over the 42 cells included in *C*. Vertical line indicates mean value.

Table 1. Block by specific Kv1 peptides

	% peak current	% at 200 ms
α-DTX (100 nM)	11.1 ± 5.1 (42)	8.8 ± 5.1(42)
DTX-K (10 nM)	4.3 ± 3.0 (5)	4.1 ± 3.0 (5)
DTX-K (100 nM)	5.4 + 3.0 (8)	5.1 ± 2.9 (8)
δ-DTX (10 nM)	4.2 ± 0.7 (3)	4.2 ± 0.7 (3)
TiTX (100 nm)	7.3 ± 3.1 (8)	5.1 ± 2.1 (8)
MTX (1 nM)	4.2 ± 2.0 (7)	3.8 ± 2.1 (7)
MTX (30 nm)	8.7 ± 4.0 (5)	5.6 ± 5.0 (5)
DTX-K (10 nM) + TiTX (100 nM)	9.2 ± 3.3 (3)	8.7 ± 3.3 (3)
MTX (1 nM) + α-DTX (500 nM)	9.5 ± 2.6 (7)	8.8 ± 2.5 (7)
α-DTX (500 nM) + MTX (1 nM)	9.8 ± 1.6 (4)	7.3 ± 1.7 (4)
DTX-K (10 nM) + α-DTX (500 nM)	15.1 ± 4.4 (3)	13.0 ± 4.2 (3)

Fig. 4*C*). Increasing the dose of α-DTX to 500 nM resulted in no additional block (7.1 ± 3.9% at 200 ms; $n = 11$).

The α-DTX-sensitive currents varied in the amount of inactivation over the 200 ms step. In 13/42 cells (31%), the α-DTX-sensitive current showed little or no inactivation ($\leq$ 10%; Fig. 4*D* and *E*). In the remaining 29 cells (69%), the α-DTX-sensitive current had both transient and persistent components (Fig. 4*D* and *E*). There appears to be a continuum of inactivation, with most cells inactivating by 10–40% (median 23.5%: Fig. 4*E*). These data suggest diversity in the functional expression of Kv1 α subunits in these cells.

The amplitude of the α-DTX-sensitive conductance (G) at 200 ms did not vary significantly with whole cell capacitance ($P = 0.21$; Fig. 5*A*1). Density of α-DTX-sensitive conductance (estimated as G/C_m) decreased with cell size (as measured by C_m: $r = -0.66$, $P < 0.0001$) (Fig. 5*A*2). In contrast, the remaining α-DTX-insensitive G increased in amplitude with increasing C_m ($r = 0.6$, $P < 0.0001$), resulting in no change in density with cell size ($P = 0.66$: Fig. 5*B*). C_m, G, and density did not vary with animal age over the range examined (P20–P36, data not shown).

Other peptide toxins. Several peptide toxins have been well characterized as specific blockers of individual Kv1 subunits (Grissmer *et al.* 1994; Koch *et al.* 1997; Harvey, 1997; Southan & Robertson, 2000; Hatton *et al.* 2001; Harvey & Robertson, 2004). In at least some cases, only a single subunit is required in a heteromultimeric channel to allow block (Hopkins, 1998; Wang *et al.* 1999; Harvey, 2001). We next tested whether there was current sensitive to peptide toxins specific for Kv1.1 (dendrotoxin-K, δ-dendrotoxin: Robertson *et al.* 1996; Wang *et al.* 1999), Kv1.2 (r-tityustotoxin-Kα: Matteson & Blaustein, 1997; Hopkins, 1998), or Kv1.3 (r-margitoxin: Garcia-Calvo *et al.* 1993) (Table 1).

We first tested the Kv1.1-specific toxin, dendrotoxin-K (DTX-K) (10 nM; K_D ~5 nM: Owen *et al.* 1997). Current

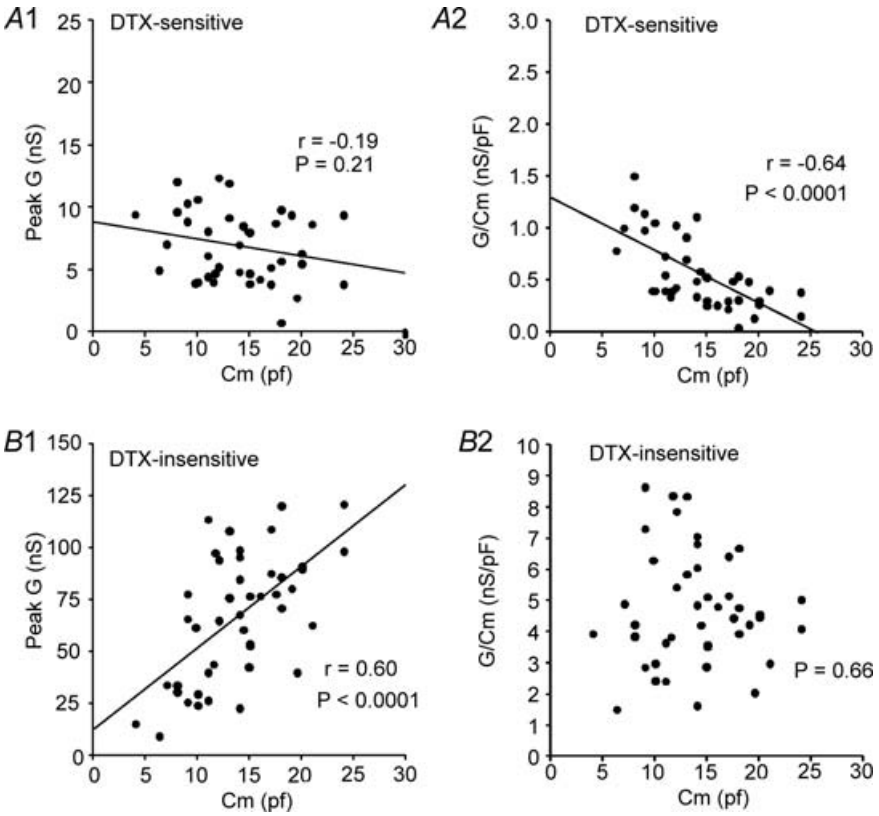

Figure 5. Plots of conductance (*G*) and current density (current divided by whole cell capacitance) *versus* whole cell capacitance
A, DTX-sensitive. *A*1, the peak *G* for the DTX-sensitive current (step to +20 or +30 mV from −70 mV) did not vary with cell size (as estimated by whole cell capacitance: C_m). *G* was determined by dividing current (at 200 ms) by driving force ($E - E_K$). *A*2, plot of current density (conductance (*G*) divided by C_m) *versus* C_m. The density of DTX-sensitive current declined with cell size (C_m). *B*, remaining DTX-insensitive component. *B*1, the DTX-insensitive conductance increased with cell size. *B*2, the DTX-insensitive current density did not vary with cell size.

was rapidly blocked ($\tau = 8.7 \pm 7.7$ s) in 5 of 5 cells tested (Table 1, Fig. 6*A–C*). In all cases, the resulting current had rapid and very slow components to activation and was persistent (Fig. 6*A*). Similar data were obtained with another Kv1.1-selective toxin, 10 nM δ-dendrotoxin ($\tau = 7.4 \pm 8.9$ s, $n = 3$). When DTX-K was tested at 100 nM (the K_D of this toxin for Kv1.2; for Kv1.1: 0.1 nM; Harvey, 2001), additional current was blocked ($n = 8$). In 3/8 cells, a transient, rapidly activating component was also present (Fig. 6*A*, lower). It has been shown that DTX-K slows activation and inactivation of Kv1.1 channels in expression systems (Robertson *et al.* 1996). It is likely, therefore, that the slow kinetics of the subtracted currents do not reflect true physiological properties of the Kv1.1-containing channels.

We next examined the effects of the selective Kv1.2 peptide r-tityustotoxin-Kα (TiTX; K_D ~0.2 nM: Werkman *et al.* 1993). TiTX rapidly blocked ($\tau = 3.3 \pm 2.6$ s) current in all 8 cells tested (Fig. 6*D–F*). In two of eight cells, the TiTX-sensitive current was rapidly activating and persistent (Fig. 6*D* and *F*). In the other six cells, there were both persistent and transient components to the current (Fig. 6*D* and *F*).

The Kv1.3-selective peptide r-margatoxin (MTX: K_D ~30 pM: Garcia-Calvo *et al.* 1993) at 1 nM blocked current ($\tau = 14.8 \pm 2.5$ s) in seven cells tested (Fig. 7*A–C*). There

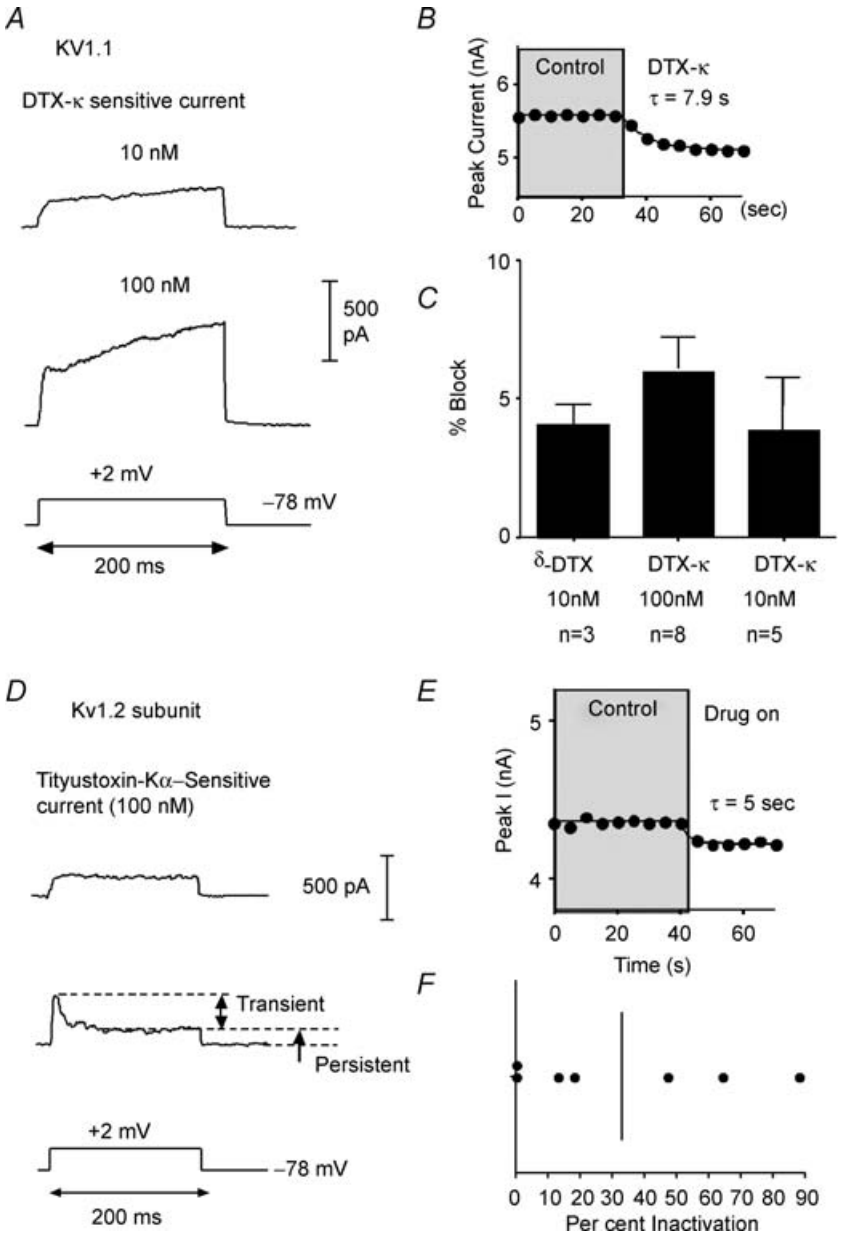

Figure 6. Specific peptide toxins for Kv1.1 and Kv1.2
A, representative traces for current sensitive to dendrotoxin-K (DTX-K) at 10 nM (upper) and 100 nM (lower). Note initial fast activation and subsequent slow rise of current with time. *B*, plot of peak current *versus* time illustrating that DTX-K onset was rapid. *C*, bar graph (mean ± S.D.) illustrating the percentage of whole cell current (at 200 ms) blocked by DTX-K or δ-DTX. *D*, representative traces for current blocked by the Kv1.2-specific toxin, r-tityustoxin-Kα (TiTX). The upper trace was from a cell where the TiTX activated rapidly and inactivated very little over the 200 ms test step. The lower trace is from a cell where both transient and persistent components of the TiTX-sensitive current were present. *E*, plot of peak current *versus* time showing that the TiTX block was rapid in onset. *F*, scatter plot of percent inactivation for 7 cells tested with TiTX (10 nM). Vertical line = mean value.

was additional block by 30 nM MTX (Table 1). The MTX-sensitive current activated rapidly and inactivated by 44 ± 29% ($n = 5$) over the 200 ms step (τ_{inact}: 92 ± 60 ms; $n = 5$) (Fig. 7*A*).

If all of the expressed Kv1 subunits formed heteromultimeric channels containing all subunit types (cf. Shamotienko *et al.* 1997; Coleman *et al.* 1999) and the presence of a single α-subunit confers toxin sensitivity on the resulting channels (Harvey, 2001), we would expect that (i) the amount of current blocked should be similar for all of the specific toxins, (ii) addition of a second toxin should result in no further block after a saturating dose of the first toxin, and (iii) the order in which toxins were applied should not matter. The amount of current blocked by application of DTX-K (Kv1.1), TiTX (Kv1.2), or MTX (Kv1.3) was similar (~3–5% of current) (Table 1). In contrast α-DTX, which affects Kv1.1, 1.2 and 1.6, blocked a greater amount of current (Table 1). These data suggest that only a fraction of the α-DTX-sensitive channels contain both Kv1.1 and Kv1.2 subunits.

If DTX-K and TiTX-sensitive currents were completely independent, one would expect 9.2% block when both toxins are added together (4.1% plus 5.1%: Table 1). In three cells, we applied 10 nM DTX-K (blocked 3.9 ± 3.6%), followed by 100 nM TiTX. In every cell, TiTX blocked additional current and the combined block was 8.7 ± 3.3% (similar to block by α-DTX alone: Table 1, Fig. 7*D*). These data suggest only partial overlap of Kv1.1 and Kv1.2 subunits in the same channels.

A similar result was obtained when 1 nM MTX was applied to eight cells (block = 3.8 ± 2.1%), followed by 500 nM α-DTX. In every cell, additional current was blocked (Fig. 7*E*), for a combined block of 7.2 ± 3.3%. This compares to an expected 13.9% block (Table 1), if MTX- and α-DTX-sensitive currents were completely independent. When we added 500 nM α-DTX first, we obtained a block of 4.0 ± 1.6% ($n = 4$) (Fig. 7*F*). Addition of margatoxin to cells previously exposed to α-DTX resulted in additional block of 2.5 ± 0.7%, for a total of 7.4 ± 1.7% block (Fig. 7*F*). These data suggest that (1) not all channels containing Kv1.1 or 1.2 subunits (α-DTX-sensitive) also contain Kv1.3 subunits, and (2) while some Kv1.3 channels are combined with Kv1.1, 1.2 or 1.6, some Kv1.3 subunits are not.

Biophysical properties of the α-DTX-sensitive current. Taken together, the previous data indicate that individual layer II/III pyramidal neurones express multiple Kv1 subunits in the soma-dendritic compartment and the expression of these subunits varies across the pyramidal cell population. In order to gain insight into the functional

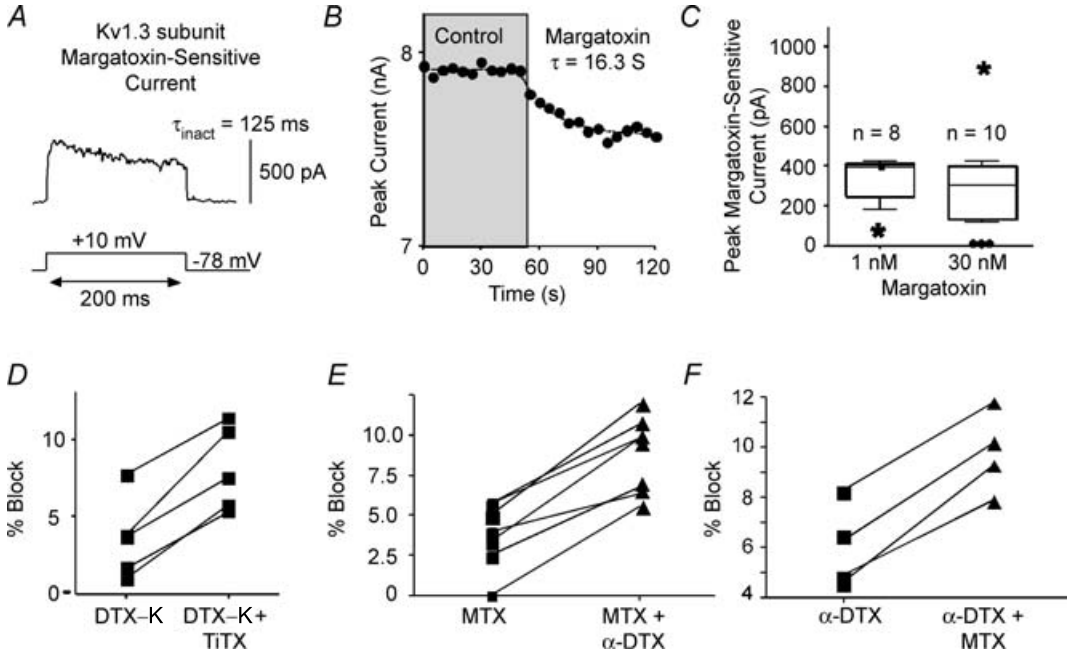

Figure 7. Specific peptide toxin for Kv1.3 and combined toxins
A, representative trace for current sensitive to r-margatoxin (MTX). *B*, plot of peak current *versus* time indicating the rate of block by MTX. *C*, box plots illustrating the distribution of responses to 1 nM or 30 nM MTX. *D–F*, scatter plots indicating response of cells to combinations of toxins. *D*, in these cells, DTX-K (10 nM) initially blocked current. In all cells, additional current was blocked by the combination of DTX-K and TiTX (100 nM). *E*, MTX (1 nM) blocked current. In all cases, α-DTX (500 nM) blocked additional current. *F*, α-DTX (500 nM) blocked current. In all cases, additional current was blocked by the combination of α-DTX plus MTX (1 nM).

consequences of Kv1 expression, we next examined the voltage dependence and kinetics of activation and inactivation of currents sensitive to 100 nM α-DTX.

Activation/deactivation. We studied steady-state activation of the α-DTX-sensitive current with a series of voltage steps (200 ms) from a holding potential of −70 or −78 mV to various potentials (Fig. 8). A typical example is shown in Fig. 8*A*–*C*. In this cell, the α-DTX-sensitive current included a transient component. The following analysis was performed for the current measured at the end of the 200 ms step. We converted current to conductance using Ohm's law and assuming driving force as test voltage minus the reversal potential. Plots of conductance *versus* voltage were fitted with a Boltzmann relationship of the form:

$$G/G_{\max} = 1/\{1 + \exp[-(V_m - V_{1/2})/V_c]\}$$

Where $V_{1/2}$ was the voltage at which 50% of maximal conductance was attained and V_c was the slope factor for the Boltzmann curve (Fig. 8*D*). On average, the α-DTX-sensitive current was activated at voltages depolarized to ∼−40 mV (Table 2), which is near the threshold range for action potentials in these cells (∼−43 mV: van Brederode *et al.* 2001). The average $V_{1/2}$ was −8.3 ± 7.9 mV with a slope factor of 9.3 ± 2.4 mV (Table 2; Fig. 8*F*) ($n = 34$ cells). The remaining, α-DTX-insensitive current was first observed at significantly more depolarized potentials ($P < 0.02$), and had a more depolarized $V_{1/2}$ ($P < 0.0001$) and different

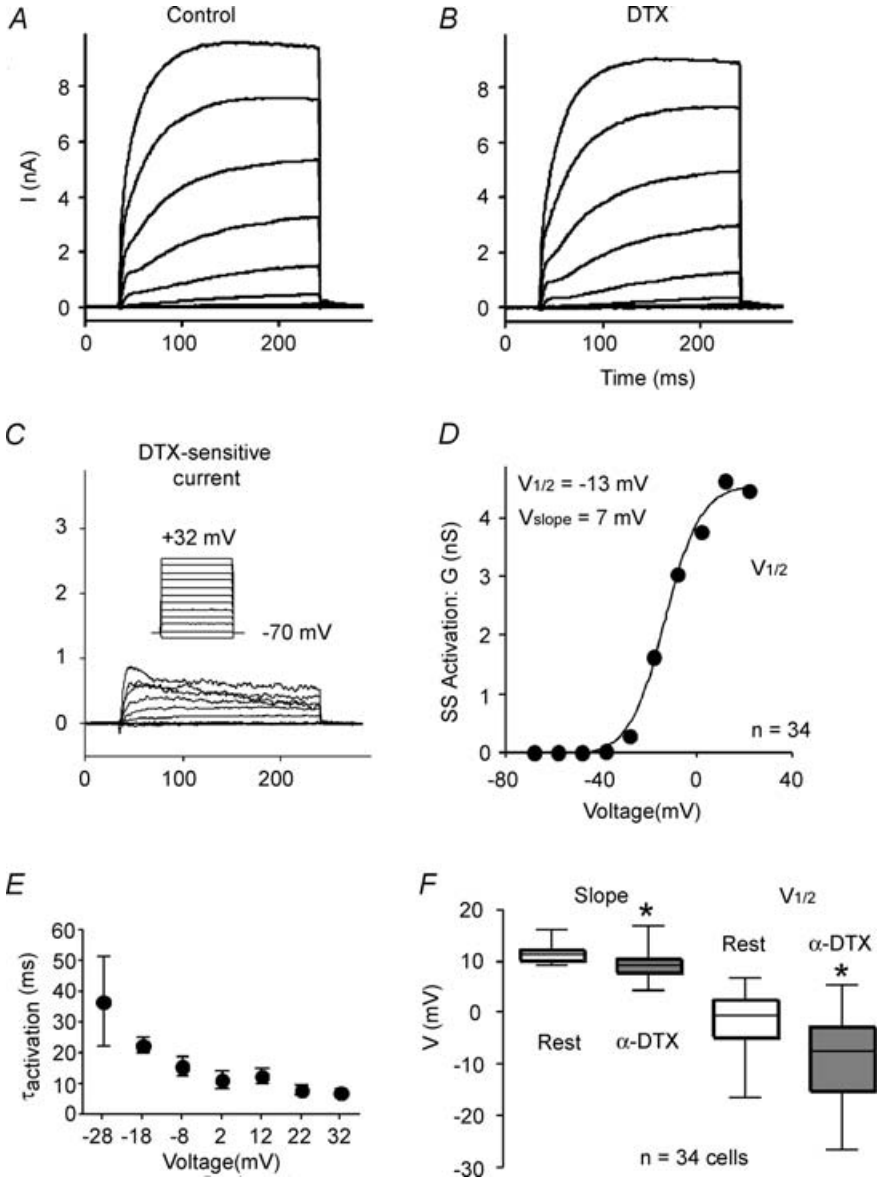

Figure 8. Activation of the α-DTX-sensitive current
A, series of current traces control solution in response to 200 ms voltage steps from −78 mV to various potentials between −70 mV and +32 mV. *B*, similar family of currents after application of 100 nM α-DTX. *C*, α-DTX-sensitive currents obtained by subtracting traces in *B* from those in *A*. Inset: voltage protocol. *D*, steady-state activation curve for cell shown in *A*–*C*. *E*, population data for activation time constant ($\tau_{activation}$) as a function of test voltage ($n = 19$ cells). *F*, box plots comparing the half-activation voltage ($V_{1/2}$) and slope for Boltzmann fits of activation curves for the α-DTX-sensitive and α-DTX-insensitive currents.

Table 2. Activation properties of the current sensitive or insensitive to α-dendrotoxin (DTX)

	G (+ 22 mV) (nS)	V for Initial Current Current (mV)	$V_{1/2,act}$† (mV)	slope (mV)	τ_{act} (+ 22 mV)†† (ms)
DTX-sensitive	8.3 ± 4.3 (34)	−40 ± 9.9 (48)	−8.3 ± 7.9 (34)	9.3 ± 2.4 (34)	4.2 ± 2.2 (19)
DTX-insensitive	58.6 ± 31.7 (34)*	−37 ± 7.3 (48)*	−1.3 ± 5.2 (34)*	11.4 ± 1.6 (34)*	27.6 ± 8.4(8)*

*Significant difference at the $\alpha = 0.05$ level.
†$V_{1/2,act}$ = Half-activation voltage.
††τ_{act} = Activation time constant.

slope factor ($P < 0.0008$) *versus* the α-DTX-sensitive current (Table 2; Fig. 8*F*).

Best fits for the kinetics of activation were obtained with an exponential raised to the 2nd or 3rd power. The exponent was greater from more negative holding potentials, suggesting multiple voltage-dependent closed state transitions (cf. Rothman & Manis, 2003*b*). The time constants were also voltage dependent, varying from ∼37 ms at −28 mV to 7–10 ms at voltages depolarized to 0 mV (Fig. 8*E*). The time constant of activation did not differ significantly as a function of holding potential. Importantly, activation was relatively slow (long τ) at voltages traversed by interspike intervals or near the voltage threshold for APs.

Tail currents were elicited by brief voltage steps (140 ms) to +10 mV from a holding potential of −70 mV (Fig. 9). The voltage was then stepped back to various potentials and current amplitude was measured at 50 ms after the step (Fig. 9*C*). The resulting tail currents reversed polarity at -81.7 ± 5.2 mV ($n = 11$ cells; Fig. 9*F*), compared to a calculated E_K of −84 mV in these experiments. These data indicate that the α-DTX-sensitive current was a K^+ current. The decay of these tail currents was well fitted by a single exponential. The time constants varied with voltage (∼40 ms at −40 mV and 10–20 ms at −60 mV to −80 mV; Fig. 9*E*).

Inactivation. With 200 ms steps, the α-DTX-sensitive current inactivated very little in most cells. With longer steps (2 s), inactivation was evident at more positive voltages (Fig. 10*C*). At all voltages, the time constants for inactivation were $\gg$ 2 s. Because of the slow inactivation, it was not possible to attain true steady-state with prepulses. We approximated steady-state inactivation with 5 s steps to various potentials, followed by a test step to +2 mV from the holding potential (−78 mV). The plots of normalized current *versus* voltage were well fitted by a single Boltzmann function of the form:

$$I/I_{max} = 1/\{1 + \exp[(V - V_{1/2})/V_c]\}$$

Approximately 65 ± 21% of the α-DTX-sensitive current could be inactivated by this protocol. For this component,

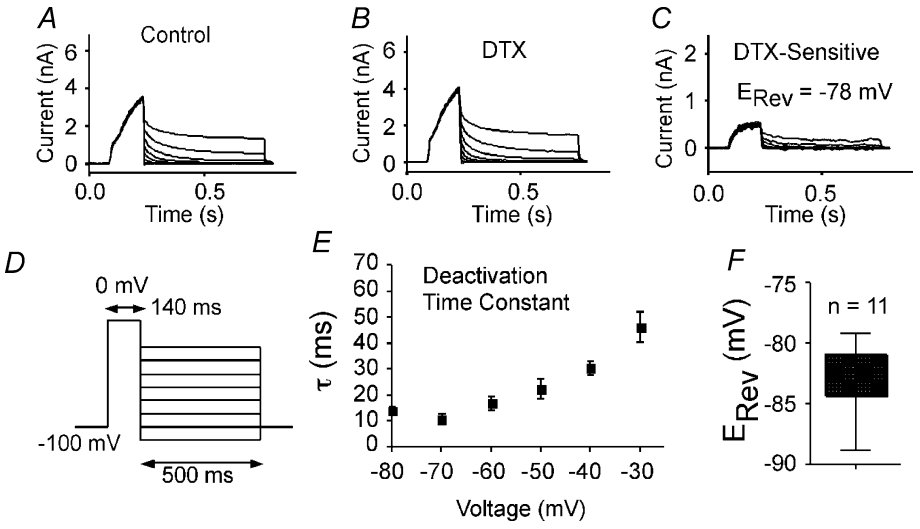

Figure 9. Deactivation of the α-DTX-sensitive current
A, control current traces in response to voltage protocol shown in *D*. *B*, similar traces after application of 100 nM α-DTX. *C*, the α-DTX-sensitive current traces (*A*–*B*). *D*, voltage protocol for *A*–*C*. *E*, population data ($n = 11$) for exponential fits to deactivation. *F*, box plots showing population data for reversal potential (obtained from protocol in *D*).

the half-inactivation voltage was -41 ± 4.4 mV and the slope factor was 5.8 ± 0.9 mV ($n = 4$ cells; Fig. 10*E*). For the remaining, α-DTX-insensitive current, this same protocol inactivated $79 \pm 9\%$ of the current ($n = 4$ cells). Both the half-inactivation voltage (-62.6 ± 4.6 mV) and slope factor (11.7 ± 3.1 mV) were significantly different from those of the α-DTX-sensitive current ($P < 0.002$ and $P < 0.03$, respectively).

As a consequence of the slow inactivation kinetics, the α-DTX-sensitive current was relatively insensitive to holding potential. The amplitude of the α-DTX-sensitive conductance was 8.2 ± 3.9 nS at -58 mV *versus* 9.4 ± 6.3 nS at -70 mV (13% change; Fig. 10*F*). In contrast the remaining α-DTX-insensitive conductance was very holding potential sensitive (47.1 ± 29.2 nS at -58 mV *versus* 80.3 ± 22.6 nS at -70 mV; 41% change: Fig. 9*G*). This results in the α-DTX-sensitive current making up a larger percentage of the whole current at more depolarized holding potentials (Fig. 10*H*). Since other components of the current inactivate much more than the α-DTX -sensitive current, the α-DTX-sensitive current is potentially much more important at membrane potentials typical for awake behaving animals (e.g. Stern *et al.* 1997; Carandini & Ferster, 2000; Steriade *et al.* 2001) than would be predicted from standard voltage-clamp experiments from negative holding potentials.

To study recovery from inactivation, we held several cells at -48 mV for > 10 s to inactivate current. Again, only a fraction of the α-DTX-sensitive current was inactivated by this protocol. Following various time periods at -100 mV, current was assessed at a test potential of 0 mV (Fig. 11). The recovery of current from inactivation of the α-DTX-sensitive current followed a single exponential of 100–1500 ms ($\tau = 431 \pm 442$ ms, $n = 10$; Fig. 11*B*). These data are again biased towards the more rapidly inactivating components of the α-DTX-sensitive current. This compares to recovery from inactivation

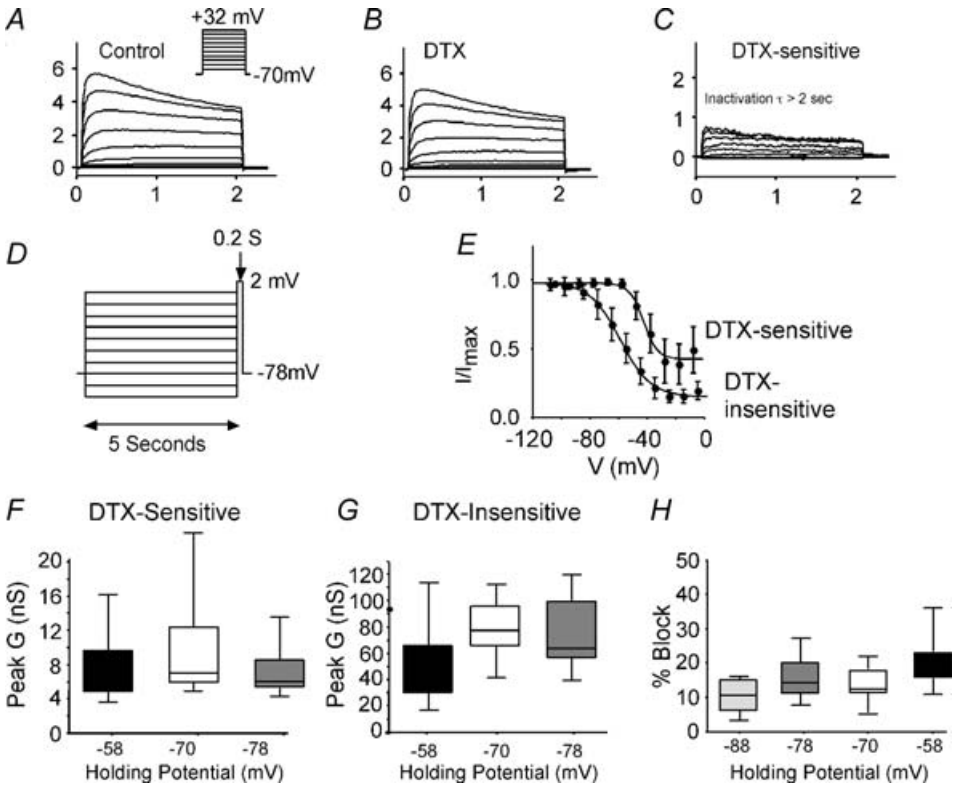

Figure 10. Inactivation of the α-DTX-sensitive current
A, time course of inactivation at various test steps (2 s in duration). Representative traces in control solution. Inset: voltage protocol for *A*–*C*. *B*, traces in presence of 100 nM α-DTX from same cell as in *A*. *C*, α-DTX-sensitive current (*A*–*B*). At all voltages τ_{inact} was > 2 s. *D*, voltage protocol for studying steady-state inactivation. *E*, population data for steady-state inactivation. The half-inactivation voltage was -48 ± 2 mV (slope 10 ± 2 mV). *F*, box plots of peak conductance (*G*) as a function of holding potential for the α-DTX-sensitive current. There were no significant differences. *G*, box plots of *G* as a function of holding potential for the α-DTX-insensitive current. Peak *G* decreased significantly at -58 mV *versus* more hyperpolarized holding potentials. *H*, the percentage of the whole current blocked by α-DTX from various holding potentials. The α-DTX-sensitive current made up a higher percentage at more depolarized holding potentials.

with a τ of 679 ± 362 ms ($n = 10$) for the remaining α-DTX-insensitive current (not significantly different from the α-DTX-sensitive current; measured at 200 ms after beginning of test step).

The α-DTX-sensitive current activates more rapidly than the persistent, α-DTX-insensitive current (Table 2).

Discussion

Our principal findings were (1) most supragranular pyramidal cells from primary somatosensory and primary motor cortex of rat express several Kv1 α subunits; (2) there is considerable variability in the subunit composition of Kv1 channels across cells; (3) the biophysical properties (e.g. amount and time course of inactivation) of the α-DTX-sensitive current vary across cells; (4) the biophysical properties of the α-DTX-sensitive current should make it more important from depolarized holding potentials, similar to resting membrane potentials in awake, behaving animals. In addition, this current should contribute to action potential voltage threshold, rheobase and regulation of firing rate.

Single cell RT-PCR revealed that individual pyramidal neurones expressed mRNA for multiple Kv1 subunits. Kv1.1 mRNA was most commonly observed, with Kv1.2, Kv1.3, and Kv1.4 also common. Kv1.5 and Kv1.6 subunit mRNAs were infrequently expressed. Our data confirm coexpression of multiple Kv1 α subunits in single cells (cf. Klumpp *et al.* 1995; Koch *et al.* 1997; Grosse *et al.* 2000; Monaghan *et al.* 2001; Alessandri-Haber *et al.* 2002; Dodson *et al.* 2002; Glazebrook *et al.* 2002; Mo *et al.* 2002; Speake *et al.* 2004).

Our immunohistochemical findings were consistent with the mRNA data and revealed some differences in cellular localization. We detected staining of the neocortical neuropil by antibodies to Kv1.1, Kv1.2, Kv1.3 and Kv1.4 subunits (but not Kv1.5 or Kv1.6; see Veh *et al.* 1995). Kv1.1, Kv1.2, Kv1.4 and Kvβ2 were predominately associated with axons and terminal fields in CA1 of the hippocampus (Monaghan *et al.* 2001).

We also observed Kv1.1, Kv1.2, Kv1.3 and Kv1.4 subunits in soma/dendritic membrane in pyramidal neurones in somatosensory and motor cortex. Typically, staining of somas and dendrites was more intense for layer V cells *versus* layer II/III and more intense in motor and cingulate cortex *versus* somatosensory cortex. Kv1.1 staining was frequently somatic, while Kv1.2 expression was more evident in proximal apical dendrites (Sheng *et al.* 1994; Wang *et al.* 1994). A novel finding in our study was intense Kv1.3 staining, seen as grape-like structures over somas and proximal dendrites. Kv1.4 staining was evident in somas and apical dendrites (Sheng *et al.* 1992). Lujan *et al.* (2003) reported that Kv1.4 expression was highest in the cerebral cortex, with diffuse staining which included somas and dendrites. Kv1.4 was observed in discrete subpopulations

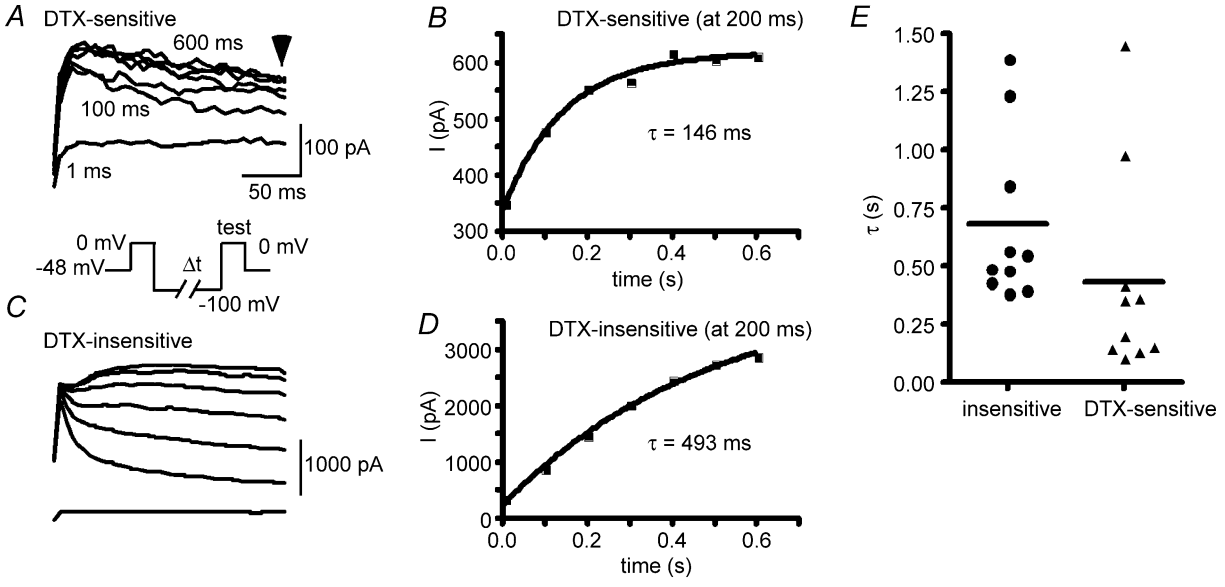

Figure 11. Recovery from inactivation
Cells were held at −40 mV for 5–10 s and then stepped to −100 mV for various times before a test pulse to 0 mV. *A*, representative traces in response to second voltage step ('test' in protocol in inset) for α-DTX-sensitive current (100 nM DTX). Inset: voltage protocol for *A* and *C*. *B*, plot of recovery of test pulse current amplitude for α-DTX-sensitive current (measured at 200 ms). *C*, the remaining, α-DTX-insensitive current. *D*, plot of recovery of test pulse current amplitude for remaining, α-DTX-insensitive current. *E*, scatter plots of recovery time constant for α-DTX-sensitive current and α-DTX-insensitive current. The time constants were not significantly different.

of hippocampal CA1 pyramidal cells (Maletic-Savatic *et al.* 1995; but see Tsaur *et al.* 1992; Cooper *et al.* 1998).

Whole cell recordings with application of peptide toxins specific for particular Kv1 subunits also revealed expression of multiple subunits in individual pyramidal cells and revealed variable biophysical properties of currents across cells. Most neurones tested revealed a current sensitive to α-DTX (blocks Kv1.1, Kv1.2, Kv1.6: 8–10% of total current). This current always had a substantial persistent component, whereas a transient component was variably expressed. The density of the α-DTX-sensitive current was greater in small *versus* large pyramidal cells from layers II/III. In layer V cells and striatal medium spiny neurones, α-DTX-sensitive current was reported to make up ∼6–16% of whole cell current (Korngreen & Sakmann, 2000; Bekkers & Delaney, 2001; Shen *et al.* 2004). In our earlier study (all layers combined), we observed ∼15% current sensitive to α-DTX (Foehring & Surmeier, 1993).

Kv1 subunit toxins revealed currents with distinctive biophysics. Kv1.1-specific toxins revealed persistent, slowly activating currents. The slow activation may reflect a toxin-induced effect rather than slow activation of Kv1.1 subunit-containing channels (Robertson *et al.* 1996). Most cells with a Kv1.2-selective, TiTX-sensitive current exhibited a transient current in addition to a persistent component. Current sensitive to the Kv1.3-selective toxin MTX inactivated at intermediate rates. Consistent with our MTX results, binding sites for kaliotoxin (sensitivity: Kv1.3 > Kv1.1 > Kv1.2) are found in highest density in neocortex (Mourre *et al.* 1999). In layer V cells in the slice preparation, no effect was reported for tityustoxin or margatoxin (Korngreen & Sakmann, 2000).

Expression system data suggest that all Kv1 subunits can co-assemble with one another (Isacoff *et al.* 1990; Ruppersberg *et al.* 1990; Parcej *et al.* 1992). Co-immunoprecipitation experiments further suggest that most neuronal Kv1 channels are heteromultimeric (Coleman *et al.* 1999; Sheng *et al.* 1993; Grissmer *et al.* 1994; Scott *et al.* 1994; Koch *et al.* 1997; Shamotienko *et al.* 1997). The subunit composition of heteromeric channel complexes influences the surface expression of Kv1 channels (Manganas & Trimmer, 2000).

We found that when more than one toxin was applied to a given cell, the second toxin always blocked additional current and the various toxins were incompletely additive. The distinctive biophysics of toxin-sensitive currents (e.g. distinctive rates of inactivation of Kv1.3-containing channels), and different distribution (from immunohistochemistry) of expressed subunits suggest that at least some Kv1 subunits are found in channels that exclude other Kv1 subtypes.

Kv1.2 subunits exist in channels with a rapidly inactivating component, suggesting either coexpression with Kv1.4 (for which we do not have a specific toxin) or Kvβ1 subunits (Robertson, 1997). It is thought that Kv1 subunits in cortex are usually expressed with Kvβ subunits (Parcej *et al.* 1992; Sheng *et al.* 1993; Rhodes *et al.* 1995, 1997; Shamotienko *et al.* 1997; Coetzee *et al.* 1999). In expression systems, channels formed with a single Kv1.4 subunit plus another Kv1 subunit have voltage dependence and kinetics similar to Kv1.4 alone (Po *et al.* 1993; Rettig *et al.* 1994; Heineman *et al.* 1996). In our experiments, transient currents were not seen with Kv1.1-specific toxins, except when the dose approached the K_D for Kv1.2 subunits, consistent with association of Kv1.2 (but not Kv1.1) with transient currents.

Biophysical properties

In expression systems, monomeric channels derived from Kv1 subunits typically activate rapidly (time constants between ∼15 and 40 ms), with half-activation voltages from ∼ −40 mV to −15 mV (Grissmer *et al.* 1994; Hopkins *et al.* 1994). All of the Kv1 subunits except Kv1.4 generate slowly inactivating, delayed rectifier-like currents (Grissmer *et al.* 1994; Hopkins *et al.* 1994). Half-inactivation for Kv1.1 was at −49 mV and for Kv1.2 was −37 mV (Hopkins *et al.* 1994). Kv1.1 and Kv1.2 currents are not very sensitive to holding potential. Kv1.1 inactivated slowly ($\tau > 2$ s) and Kv1.2 inactivated with a slow ($\tau > 3$ s) and a fast (τ ∼130 ms) component. Kv1.3 channels inactivated more rapidly than Kv1.1, Kv1.2 or Kv1.5 (Grissmer *et al.* 1994). Recovery from inactivation is typically slow for Kv1.1 (∼2–3 s: Hopkins *et al.* 1994). Recovery of Kv1.2 had fast (∼300 ms) and slow (∼2 s) components of recovery (Hopkins *et al.* 1994).

We determined the biophysical properties of the α-DTX-sensitive current in layer II/III pyramidal neurones. Our measurements concentrated on the persistent component (at the end of 200 ms test steps). The α-DTX-sensitive currents reversed at near E_K, indicating that they were K^+ currents.

Activation/deactivation

Several neurone types in the auditory system express large α-DTX-sensitive currents that activate in the subthreshold voltage range and exert powerful control over spiking (Dodson *et al.* 2002; Brew *et al.* 2003). In cells from the medial nucleus of the trapezoid body (MNTB), DTX-I-sensitive current makes up > 80% of the outward current (Dodson *et al.* 2002). In the MNTB and ventral cochlear nucleus, α-DTX-sensitive current activated rapidly above −70 to −60 mV with a $V_{1/2}$ of ∼ −50 mV (Brew & Forsythe, 1995; Macica *et al.* 2003; Dodson *et al.* 2002; Rothman & Manis, 2003*b*).

Activation of the α-DTX-sensitive current also occurs at subthreshold voltages in layer V neocortical pyramidal neurones (Bekkers & Delaney, 2001), striatal medium spiny neurones (Shen *et al.* 2004), and nodose ganglia (Glazebrook *et al.* 2002). In layer V pyramidal cells, the half-activation voltage for the α-DTX-sensitive current was −22 mV (Bekkers & Delaney, 2001). The α-DTX-sensitive current was observed at voltages positive to ∼ −55 mV and inactivated slowly. In medium spiny neurones, the α-DTX-sensitive current activation $V_{½}$ was −27 mV (Shen *et al.* 2004).

We found that the α-DTX-sensitive current in layer II/III pyramidal neurones was first observed at significantly more negative potentials than the remaining, DTX-insensitive current (see also Rothman & Manis, 2003*a*), but more depolarized than the cell types discussed above ($V_{½}$ of −8 mV). The foot of the activation curve (∼ −40 mV) was near the threshold for action potentials in these neurones (−43 mV; van Brederode *et al.* 2000). There was considerable variability in the onset voltage across cells. In some pyramidal cells activation is clearly subthreshold whereas in other cells activation occurs at more depolarized voltages. Activation of the α-DTX-sensitive current was voltage dependent, being slower at the foot of the activation curve and faster at depolarized potentials. The α-DTX-sensitive current activated faster than the remaining, α-DTX-insensitive current at all potentials.

In mouse CA1 pyramidal neurones, the α-DTX-sensitive current was also first evident depolarized to ∼ −40 mV (Wu & Barish, 1992). In amygdaloid pyramidal neurones, the α-DTX-sensitive current activated rapidly and inactivated slowly (Faber & Sah, 2004). The activation threshold was −33 mV and $V_{½}$ was ∼ +5 mV (slope: 13 mV) (Faber & Sah, 2004). In these cells the α-DTX-sensitive current was located exclusively on the proximal apical dendrite. Thus layer II/III cells, like CA1 and amygdaloid pyramidal cells, express α-DTX-sensitive channels which activate in the near-threshold voltage range, rather than clearly subthreshold as in layer V cells, medium spiny neurones, and auditory cells.

Even though the current sensitive to α-DTX made up a small percentage of the total possible current in layer II/III pyramidal neurones, because of the relatively hyperpolarized voltages at which this current activates, the α-DTX-sensitive current makes up a larger percentage of the current at negative test voltages (−40 to −20 mV). The fast activation kinetics (Table 2) also allow the α-DTX-sensitive current to contribute a high proportion of the current at early times after the step. Deactivation τ values were also voltage dependent in layer II/III pyramidal cells and were relatively slow at voltages corresponding to *in vivo* resting potentials and potentials traversed by interspike intervals during repetitive firing.

Inactivation/recovery

The degree to which the α-DTX-sensitive current inactivated in layer II/III pyramidal neurones was highly variable between cells. Presumably this reflects differences between cells in the composition of α and β subunits of Kv1 channels, although we cannot completely rule out contributions from voltage dependence of toxin block, location of channels, or series resistance. There was always a persistent current component, towards which our analyses are biased. The half-inactivation voltage for the α-DTX-sensitive current (−41 mV) was significantly more depolarized than that for the remaining α-DTX-insensitive current (−63 mV).

In CA1 pyramidal cells, the α-DTX-sensitive current inactivated slowly and the half-inactivation voltage was −22 mV (Wu & Barish, 1992). This compares to half-inactivation at −88 mV for the 4-AP-sensitive D current described by Storm (1988) in rat CA1 pyramidal cells. The time constant for recovery from inactivation in CA1 varied between 80 and 200 ms (between −120 mV and −60 mV; Wu & Barish, 1992) *versus* tens of seconds in Storm (1988).

As a consequence of its inactivation voltage dependence and kinetics, the α-DTX-sensitive current in layer II/III pyramidal cells was relatively insensitive to holding potential. This suggests that this component would be relatively more important from holding potentials similar to resting potentials observed for awake, behaving animals (∼ −50 mV for cortex in the 'up' state; Stern *et al.* 1997) as compared to estimates from quiescent cells *in vitro* (or 'down state' *in vivo*: negative to −60 mV; Stern *et al.* 1997).

In contrast to cortex, the α-DTX-sensitive current in medium spiny neurones was very holding potential sensitive (block changed from 15% from −90 mV to 9% from −60 mV; Shen *et al.* 2004), and recovery from inactivation was slow (τ ∼1 s at −100 mV). In MNTB neurones, the half-inactivation was estimated as ∼ −50 mV, with only about 40% of current inactivating (Dodson *et al.* 2002). In neurones from the lateral cochlear nucleus, inactivation was slow (τ > 150 ms) and recovery from inactivation rapid (τ = 54 ms: Rothman & Manis, 2003*b*).

The general pattern of biophysical properties in different cell types may correspond to the relative expression of different Kv1 subunits. Cell types with the most hyperpolarized activation and inactivation (e.g. auditory nuclei) appear to be dominated by Kv1.1 or Kv1.1/1.2 heteromeric channels (Dodson *et al.* 2002). Cell types with the most depolarized activation range (e.g. amygdaloid pyramidal neurones) appear to mainly express Kv1.2 subunits (Faber & Sah, 2004). Neocortical pyramidal cells express many Kv1 subunits in soma/dendritic channels and have intermediate voltage dependence.

The 'D' current

Current usage equates α-DTX sensitivity with the 'D' current and activation and inactivation properties of the α-DTX-sensitive current varies between cell types and laboratories. It has been suggested that D current may be due to Kv1.2 subunits plus a Kvβ (Coetzee *et al.* 1999). Storm (1988) originally coined the term 'D current' from recordings in CA1 pyramidal neurones as a highly 4-AP-sensitive current that inactivated slowly and was very sensitive to holding potential. This current activated in the subthreshold range and endowed a slow ramp voltage response up to spike threshold (in response to stimulation from negative holding potentials). The α-DTX-sensitive current in layer II/III cells also activates in the near threshold voltage range and inactivates slowly, but is much different from the current described by Storm in that the neocortical current is not holding-potential sensitive. Our current has biophysical properties similar to α-DTX-sensitive currents in CA1 (Wu & Barish, 1992), but unlike the classical D current.

Predictions for function

Our data suggest that the α-DTX-sensitive current should not contribute to resting potential and should not have significant effects on AP repolarization (small percentage of current) after stimulation from negative resting potentials. The α-DTX-sensitive current is also likely to be more important at the depolarized holding potentials in awake behaving animals (Cowan & Wilson, 1994; Stern *et al.* 1997; Steriade *et al.* 2001). Since the α-DTX-sensitive current activates around the threshold voltage range, it should influence rheobase and voltage threshold, especially in response to slow or long lasting stimuli. The slow kinetics of deactivation at ~ -50 mV suggest that the α-DTX-sensitive current should influence interspike intervals and firing rate.

References

Alessandri-Haber N, Alcaraz G, Deleuze C, Jullien F, Manrique C, Couraud F, Creste M & Giraud P (2002). Molecular determinants of emerging excitability in rat embryonic motoneurons. *J Physiol* **541**, 25–39.

Baldwin TJ, Tsaur M-L, Lopez GA, Jan YN & Jan LY (1991). Characterization of a mammalian cDNA for an inactivating voltage-sensitive K^+ channel. *Neuron* **7**, 471–483.

Bekkers JM & Delaney AJ (2001). Modulation of excitability by α-dendrotoxin-sensitive potassium channels in neocortical pyramidal neurons. *J Neurosci* **21**, 6553–6560.

Bossu J-L & Gähwiler BH (1996). Distinct modes of channel gating underlie inactivation of somatic K^+ current in rat hippocampal pyramidal cells *in vitro*. *J Physiol* **495**, 383–397.

Brew HM & Forsythe ID (1995). Two voltage-dependent K^+ conductances with complementary functions in postsynaptic integration at a central auditory synapse. *J Neurosci* **15**, 8011–8022.

Brew HM, Hallows JL & Tempel BL (2003). Hyperexcitability and reduced low threshold potassium currents in auditory neurons of mice lacking the channel subunit Kv1.1. *J Physiol* **548**, 1–20.

Carandini M & Ferster D (2000). Membrane potential and firing rate in cat primary visual cortex. *J Neurosci* **20**, 470–484.

Castellino RC, Morales MJ, Strauss HC & Rasmusson RL (1995). Time- and voltage-dependent modulation of a Kv1.4 channel by a beta-subunit (Kvβ3) cloned from ferret ventricle. *Am J Physiol* **269**, H385–H391.

Chen X & Johnston D (2004). Properties of single voltage-dependent K^+ channels in dendrites of CA1 pyramidal neurons of rat hippocampus. *J Physiol* **559**, 187–203.

Coetzee WA, Amarillo Y, Chiu J, Chow A, Lau D, McCormack T, Moreno H, Nadal MS, Ozalta A, Pountey F, Saganich M, Vega Saenz De Miera E & Rudy B (1999). Molecular diversity of K^+ channels. *Ann NY Acad Sci* **868**, 233–285.

Coghlan MJ, Carroll WA & Gopalkrishnan M (2001). Recent developments in the biology and medicinal chemistry of potassium channel modulators: update from a decade of progress. *J Med Chem* **44**, 1627–1653.

Coleman SK, Newcombe J, Pryke J & Dolly JO (1999). Subunit composition of Kv1 channels in human CNS. *J Neurochem* **73**, 849–858.

Cooper EC, Milroy A, Jan YN, Jan LY & Lowenstein DH (1998). Presynaptic localization of Kv1.4-containing A-type potassium channels near excitatory synapses in the hippocampus. *J Neurosci* **18**, 965–974.

Cowan RL & Wilson CJ (1994). Spontaneous firing patterns and axonal projections of single corticostriatal neurons in the rat medial agranular cortex. *J Neurophysiol* **71**, 17–32.

Dodson PD, Barker MC & Forsythe ID (2002). Two heteromeric Kv1 potassium channels differentially regulate action potential firing. *J Neurosci* **22**, 6953–6961.

Dodson PD, Billups B, Rusznak Z, Szucs G, Barker MC & Forsythe ID (2003). Presynaptic rat Kv1.2 channels suppress synaptic terminal hyperexcitability following action potential invasion. *J Physiol* **550**, 27–33.

Dong Y & White FJ (2003). Dopamine D1-class receptors selectively modulate a slowly inactivating potassium current in rat medial prefrontal cortex. *J Neurosci* **23**, 2686–2695.

Drewe JA, Verma S, Frech G & Joho R (1992). Distinct spatial and temporal expression patterns of K^+ channel mRNAs from different subfamilies. *J Neurosci* **12**, 538–548.

Faber ES & Sah P (2004). Opioids inhibit lateral amygdala pyramidal neurons by enhancing a dendritic potassium current. *J Neurosci* **24**, 3031–3039.

Foehring RC & Surmeier DJ (1993). Voltage-gated potassium currents in acutely dissociated rat cortical neurons. *J Neurophysiol* **70**, 51063.

Garcia-Calvo M, Leonard RJ, Novick J, Stevens SP, Schmalhofer W, Kaczorowski GJ & Garcia ML (1993). Purification, characterization, and biosynthesis of margatoxin, a component of *Centuroides margaritus* venom that selectively inhibits voltage-dependent potassium channels. *J Biol Chem* **268**, 18866–18874.

Glazebrook PA, Ramirez AN, Schild JH, Shieh CC, Doan T, Wible BA & Kunze DL (2002). Potassium channels Kv1.1, Kv1.2, and Kv1.6 influence excitability of rat visceral sensory neurons. *J Physiol* **541**, 467–482.

Grissmer S, Nguyen AN, Aiyar J, Hanson DC, Mather RJ, Gutman GA, Karmilowicz MJ, Auperin DD & Chandy KG (1994). Pharmacological characterization of five cloned voltage gated K channels, types Kv1.1, 1.2, 1.3, 1.5, 3.1, stably expressed in mammalian cell lines. *Mol Pharmacol* **45**, 1227–1234.

Grosse G, Draguhn A, Hohne L, Tapp R, Veh RW & Ahnert-Hilger G (2000). Expression of Kv1 potassium channels in mouse hippocampal primary cultures. development and activity-dependent regulation. *J Neurosci* **20**, 1869–1882.

Halliwell JV, Othman IB, Pelchen-Matthews A & Dolly JO (1986). Central action of dendrotoxin: selective reduction of a transient K^+ conductance in hippocampus and binding to localized acceptors. *Proc Natl Acad Sci* **83**, 493–497.

Harvey AL (1997). Recent studies on dendrotoxins and potassium ion channels. *General Pharmacol* **28**, 7–12.

Harvey AL (2001). Twenty years of dendrotoxins. *Toxicon* **39**, 15–26.

Harvey AL & Robertson B (2004). Dendrotoxins. Structure-function relationships and effects on potassium ion channels. *Curr Med Chem* **11**, 3065–3072.

Hatton MJ, Mason HS, Carl A, Doherty P, Latten MJ, Kenyon JL, Sanders KM & Horowitz B (2001). Functional and molecular expression of a voltage-dependent K^+ channel (Kv1.1) in interstitial cells of Cajal. *J Physiol* **533**, 315–327.

Heineman SH, Rettig J, Graack HR & Pongs O (1996). Molecular and functional characterization of Kv channel β-subunits from rat brain. *J Physiol* **493**, 625–633.

Hopkins WF (1998). Toxin and subunit specificity of blocking affinity of three peptide toxins for heteromultimeric, voltage-gated potassium channels expressed by *Xenopus* oocytes. *J Pharmacol Exp Ther* **285**, 1051–1060.

Hopkins WF, Allen ML, Houamed KM & Tempel BL (1994). Properties of voltage-gated K^+ currents expressed in *Xenopus* oocytes by mKv1.1, mKv1.2 and their heteromultimers as revealed by mutagenesis of the dendrotoxin-binding site in mKv1.1. *Pflugers Arch* **428**, 382–390.

Hwang PM, Glatt CE, Bredt DS, Yellen G & Snyder SH (1992). A novel K^+ channel with unique localizations in mammalian brain. Molecular cloning and characterization. *Neuron* **8**, 473–481.

Isacoff EY, Jan YN & Jan LY (1990). Evidence for the formation of heteromultimeric potassium channels in *Xenopus* oocytes. *Nature* **345**, 530–534.

Jan LY & Jan YN (1992). Structural elements involved in specific K^+ channel function. *Annu Rev Physiol* **54**, 537–555.

Jones EG, Huntley GW & Benson DL (1994). Alpha calcium/calmodulin-dependent protein kinase II selectively expressed in a subpopulation of excitatory neurons in monkey sensory-motor cortex: comparison with GAD-67 expression. *J Neurosci* **14**, 611–629.

Klumpp DJ, Song EJ, Ito S, Sheng M, Jan LY & Pinto LH (1995). The shaker-like potassium channels of the mouse rod bipolar cell and their contributions to the membrane current. *J Neurosci* **15**, 5004–5013.

Koch RO, Wanner SG, Koschak A, Hanner M, Schwarzer C, Kacrowski GJ, Slaughter RS, Garcia ML & Knauss HG (1997). Complex subunit assembly of neuronal voltage-gated K^+ channels. *J Biol Chem* **272**, 27577–27581.

Korngreen A & Sakmann B (2000). Voltage-gated K^+ channels in layer 5 neocortical pyramidal neurons from young rats. subtypes and gradients. *J Physiol* **525**, 621–639.

Locke RE & Nerbonne JM (1997). Role of voltage-gated K^+ currents in mediating the regular-spiking phenotype of callosal-projecting rat visual cortical neurons. *J Neurophysiol* **78**, 2321–2335.

Lujan R, de Cabo de la Vega C, Dominguez del Toro E, Ballesta JJ, Criado M & Juiz JM (2003). Immunohistochemical localization of the voltage-gated potassium channel subunit Kv1.4 in the central nervous system of the adult rat. *J Chem Neuroanat* **26**, 209–224.

Macica CM, von Hehn CA, Wang LY, Ho CS, Yokoyama S, Joho RH & Kaczmarek LK (2003). Modulation of the kv3.1b potassium channel isoform adjusts the fidelity of the firing pattern of auditory neurons. *Neurosci* **23**, 1133–1141.

Owen DG, Hall A, Stephens G, Stow J & Robertson B (1997). The relative potencies of dendrotoxins as blockers of the cloned voltage-gated K^+ channel, mKv1.1 (MK-1), when stably expressed in Chinese hamster ovary cells. *Br J Pharmacol* **120**, 1029–1034.

Parcej DN, Scott VE & Dolly JO (1992). Oligomeric properties of alpha-dendrotoxin-sensitive potassium ion channels purified from bovine brain. *Biochemistry* **31**, 11084–11088.

Po S, Roberds S, Snyders DJ, Tamkun M & Bennet PB (1993). Heteromeric assembly of human potassium channels. Molecular basis of a transient outward current. *Circ Res* **2**, 1326–1336.

Pongs O (1992). Molecular biology of voltage dependent potassium channels. *Physiol Rev* **72**, S69–S88.

Rettig J, Heinemann SH, Wunder F, Lorra C, Pacej DN & Dolly OJ (1994). Inactivation properties of voltage-gated K^+ channels altered by the presence of β-subunit. *Nature* **369**, 289–294.

Rho JM, Szot P, Tempel BL & Schwartzkroin PA (1999). Developmental seizure susceptibility of Kv1.1 potassium channel knockout mice. *Dev Neurosci* **21**, 320–327.

Rhodes KJ, Keibaugh SA, Barrazueta NX, Lopez KL & Trimmer JS (1995). Association and colocalization of K^+ channel alpha- and beta-subunit polypeptides in rat brain. *J Neurosci* **15**, 5360–5371.

Rhodes KJ, Strassle BW, Monaghan MM, Bekele-Arcuri Z, Matos MF & Trimmer JS (1997). Association and colocalization of the Kvβ1 and Kvβ2 β-subunits with the Kv1 α-subunits in mammalian brain K^+ channel complexes. *J Neurosci* **17**, 8246–8258.

Robertson B (1997). The real life of voltage-gated K^+ channels: more than model behaviour. *Trends Pharmacol Sci* **18**, 474–483.

Robertson B, Owen D, Stow J, Butler C & Newland C (1996). Novel effects of dendrotoxin homologues on subtypes of mammalian Kv1 potassium channels expressed in *Xenopus* oocytes. *FEBS Lett* **383**, 26–30.

Rothman JS & Manis PB (2003*a*). Differential expression of three distinct potassium currents in the ventral cochlear nucleus. *J Neurophysiol* **89**, 3070–3082.

Rothman JS & Manis PB (2003*b*). Kinetic analyses of three distinct potassium currents in the ventral cochlear nucleus. *J Neurophysiol* **89**, 3083–3096.

Rothman JS & Manis PB (2003*c*). The roles potassium currents play in regulating the electrical activity of ventral cochlear nucleus neurons. *J Neurophysiol* **89**, 3097–3113.

Ruppersberg JP, Schroter KH, Sakmann B, Stocker M, Sewing S & Pongs O (1990). Heteromultimeric channels formed by rat brain potassium channel proteins. *Nature* **345**, 535–537.

Salkoff L, Baker K, Butler A, Covarrubias M, Pak MD & Wei A (1992). An essential 'set' of K^+ channels conserved in flies, mice and humans. *Trends Neurosci* **15**, 161–166.

Scott VES, Muniz ZM, Sewing S, Lichtenhagen R, Parcej DN, Pongs O & Dolly JO (1994). Antibodies specific for distinct Kv subunits unveil a heterooligomeric basis for subtypes of alpha-dendrotoxin-sensitive K^+ channels in bovine brain. *Biochem* **33**, 1617–1623.

Serodio P & Rudy B (1998). Differential expression of Kv4 K^+ channel subunits mediating subthreshold transient K^+ (A type) currents in rat brain. *J Neurophysiol* **79**, 1081–1091.

Shamotienko OG, Parcej DN & Dolly JO (1997). Subunit combinations defined for K^+ channel Kv1 subtypes in synaptic membranes from bovine brain. *Biochem* **36**, 8195–8201.

Shen W, Hernandez-Lopez S, Tkatch T, Held JE & Surmeier DJ (2004). Kv1.2-containing K^+ channels regulate subthreshold excitability of striatal medium spiny neurons. *J Neurophysiol* **91**, 1337–1349.

Sheng M, Liao YJ, Jan YN & Jan LY (1993). Detection of heteromultimeric K^+ channels in vivo: potential molecular basis of a presynaptic A-current. *Nature* **365**, 72–75.

Sheng M, Tsaur M-L, Jan YN & Jan LY (1992). Subcellular segregation of two A-type K^+ channel proteins in rat central neurons. *Neuron* **9**, 271–284.

Sheng M, Tsaur M-L, Jan YN & Jan LY (1994). Contrasting subcellular localization of the Kv1.2 K^+ channel subunit in different neurons of rat brain. *J Neurosci* **14**, 2408–2417.

Smart SL, Lopantsev V, Zhang CL, Robbins CA, Wang H, Chiu SY, Schwartzkroin PA, Messing AM & Tempel BL (1998). Deletion of the Kv1.1 channels causes epilepsy in mice. *Neuron* **20**, 809–819.

Song WJ, Tkatch T, Baranauskas G, Ichinohe N, Kitai ST & Surmeier DJ (1998). Somatodendritic depolarization-activated potassium currents in rat neostriatal cholinergic interneurons are predominantly of the A type and attributable to coexpression of Kv4.2 and Kv4.1 subunits. *J Neurosci* **18**, 3124–3137.

Southan AP & Robertson B (2000). Electrophysiological characterization of voltage-gated K^+ currents in cerebellar basket and purkinje cells. Kv1 and Kv3 channel subfamilies are present in basket cell nerve terminals. *J Neurosci* **20**, 114–122.

Speake T, Kibble JD & Brown PD (2004). Kv1.1 and Kv1.3 channels contribute to the delayed-rectifying K^+ conductance in rat choroid plexus epithelial cells. *Am J Physiol Cell Physiol* **286**, C611–C620.

Steriade M, Timofeev I & Grenier F (2001). Natural waking and sleep states: a view from inside neocortical neurons. *J Neurophysiol* **85**, 1969–1985.

Stern EA, Kincaid AE & Wilson CJ (1997). Spontaneous subthreshold membrane potential fluctuations and action potential variability of rat corticostriatal and striatal neurons in vivo. *J Neurophysiol* **77**, 1697–1715.

Storm JF (1988). Temporal integration by a slowly inactivating K^+ current in hippocampal neurons. *Nature* **336**, 379–381.

Stuhmer W, Ruppersberg JP, Schroter KH, Sakmann B, Stocker M, Giese KP, Perschke A, Baumann A & Pongs O (1989). Molecular basis of functional diversity of voltage gated potassium channels in mammalian brain. *EMBO J* **8**, 3235–3244.

Tsaur M-L, Sheng M, Lowenstein DH, Jan YN & Jan LY (1992). Differential expression of K^+ channel mRNAs in rat brain and down regulation in hippocampus following seizures. *Neuron* **8**, 1055–1067.

Tseng-Crank JCL, Tseng G-N, Schwartz A & Tanouye MA (1990). Molecular cloning and functional expression of a potassium channel cDNA isolated from rat cardiac library. *FEBS Lett* **268**, 63–68.

Tukey JW (1977). *Exploratory Data Analysis*. Addsion-Wesley, Reading, PA, USA.

van Brederode JF, Rho JM, Cerne R, Tempel BL & Spain WJ (2001). Evidence of altered inhibition in layer V pyramidal neurons from neocortex of Kcna1-null mice. *Neurosci* **103**, 921–929.

Veh RW, Lichtinghagen R, Sewing S, Wunder F, Grumbach IM & Pongs O (1995). Immunocytochemical localization of five members of the Kv1 channel subunits: contrasting subcellular locations and neuron-specific colocalizations in the rat brain. *Eur J Neurosci* **7**, 2189–2205.

Vysokanov A, Flores-Hernandez J & Surmeier DJ (1998). mRNAs for clozapine-sensitive receptors co-localize in rat prefrontal cortex neurons. *Neurosci Lett* **258**, 179–182.

Wang H, Kunkel DD, Martin TM, Schwartzkroin PA & Tempel BL (1993). Heteromeric K^+ channels in terminal and juxtaparanodal regions of neurons. *Nature* **365**, 75–79.

Wang H, Kunkel DD, Schwartzkroin PA & Tempel BL (1994). Localization of Kv1.1 and Kv1.2, two K channel proteins, to synaptic terminals, somata and dendrites in the mouse brain. *J Neurosci* **14**, 4588–4599.

Wang FC, Parcej DN & Dolly JO (1999). Alpha subunit compositions of Kv1.1-containing K^+ channel subtypes fractionated from rat brain using dendrotoxins. *Eur J Biochem* **263**, 230–237.

Werkman TR, Gustafson TA, Rogowski RS, Blaustein MP & Rogawski MA (1993). Tityustoxin-K alpha, a structurally novel and highly potent K^+ channel peptide toxin, interacts with the alpha-dendrotoxin binding site on the cloned Kv1.2 K^+ channel. *Mol Pharmacol* **44**, 430–436.

Wu R & Barish ME (1992). Two pharmacologically and kinetically distinct transient potassium currents in cultured embryonic mouse hippocampal neurons. *J Neurosci* **12**, 2235–2246.

Zhou F-M & Hablitz JJ (1996). Layer I neurons of the rat cortex. II. Voltage-dependent outward currents. *J Neurophysiol* **76**, 668–682.

Acknowledgements

We would like to express our gratitude to Yu Chen, Rebecca Foehring, Sharon Phillips, and Karen Saporito for excellent technical assistance. This work was funded by NINDS grant NS044163 (to R.C.F.), NS047085 (to D.J.S.) and HD41002 (to W.E.A.).